REPORT DOCUMENTATION PAGE

Form Approved
OMB No. 0704-0188

1. REPORT DATE *(DD-MM-YYYY)*	2. REPORT TYPE	3. DATES COVERED *(From - To)*
30-11-2009	REPRINT	

4. TITLE AND SUBTITLE
A technique for short-term warning of solar energetic particle events based on flare location, flare size, and evidence of particle escape

5a. CONTRACT NUMBER

5b. GRANT NUMBER

5c. PROGRAM ELEMENT NUMBER
62601F

6. AUTHOR(S).
M. Laurenza*, E.W. Cliver, J. Hewitt, M. Storini*, A.G. Ling**, C.C. Balch#, and M. L. Kaiser##

5d. PROJECT NUMBER
1010

5e. TASK NUMBER
RD

5f. WORK UNIT NUMBER
A1

7. PERFORMING ORGANIZATION NAME(S) AND ADDRESS(ES)

Air Force Research Laboratory
29 Randolph Road
Hanscom AFB MA 01731-3010

8. PERFORMING ORGANIZATION REPORT NUMBER

AFRL-RV-HA-TR-2009-1109

9. SPONSORING / MONITORING AGENCY NAME(S) AND ADDRESS(ES)

10. SPONSOR/MONITOR'S ACRONYM(S)

12. DISTRIBUTION / AVAILABILITY STATEMENT
Approved for Public Release; Distribution Unlimited

13. SUPPLEMENTARY NOTES
REPRINTED FROM: SPACE WEATHER, VOL 7, S04008, doi: 10.1029/2007SW000379, 2009
 - *INAF, Rome, Italy, **AER, Lexington, MA(continued on reverse)

14. ABSTRACT

[1] We have developed a technique to provide short-term warnings of solar energetic proton (SEP) events that meet or exceed the Space Weather Prediction Center threshold of J (>10 MeV) = 10 pr cm^{-2} s^{-1} sr^{-1}. The method is based on flare location, flare size, and evidence of particle acceleration/escape as parameterized by flare longitude, time-integrated soft X-ray intensity, and time-integrated intensity of type III radio emission at ~1 MHz, respectively. In this technique, warnings are issued 10 min after the maximum of ≥M2 soft X-ray flares. For the solar cycle 23 (1995–2005) data on which it was developed, the method has a probability of detection of 63% (47/75), a false alarm rate of 42% (34/81), and a median warning time of ~55 min for the 19 events successfully predicted by our technique for which SEP event onset times were provided by Posner (2007). These measures meet or exceed verification results for competing automated SEP warning techniques but, at the present stage of space weather forecasting, fall well short of those achieved with a human (aided by techniques such as ours) making the ultimate yes/no SEP event prediction. We give some suggestions as to how our method could be improved and provide our flare and SEP event database in the auxiliary material to facilitate quantitative comparisons with techniques developed in the future.

15. SUBJECT TERM
Solar energetic protons Short-term warnings X-ray flares

16. SECURITY CLASSIFICATION OF:			17. LIMITATION OF ABSTRACT	18. NUMBER OF PAGES	19a. NAME OF RESPONSIBLE PERSON
a. REPORT	b. ABSTRACT	c. THIS PAGE			Donald Norquist
UNCLAS	UNCLAS	UNCLAS	SAR		19b. TELEPHONE NUMBER *(include area code)*

Continuation No. 13

#NOAA, Space Weather Prediction Center, Boulder, CO
##NASA Goddard Space Flight Center, Greenbelt, MD

SPACE WEATHER, VOL. 7, S04008, doi:10.1029/2007SW000379, 2009

A technique for short-term warning of solar energetic particle events based on flare location, flare size, and evidence of particle escape

M. Laurenza,[1] E. W. Cliver,[2] J. Hewitt,[2] M. Storini,[1] A. G. Ling,[3] C. C. Balch,[4] and M. L. Kaiser[5]

Received 23 December 2007; revised 13 October 2008; accepted 18 October 2008; published 30 April 2009.

[1] We have developed a technique to provide short-term warnings of solar energetic proton (SEP) events that meet or exceed the Space Weather Prediction Center threshold of J (>10 MeV) = 10 pr cm^{-2} s^{-1} sr^{-1}. The method is based on flare location, flare size, and evidence of particle acceleration/escape as parameterized by flare longitude, time-integrated soft X-ray intensity, and time-integrated intensity of type III radio emission at ~1 MHz, respectively. In this technique, warnings are issued 10 min after the maximum of ≥M2 soft X-ray flares. For the solar cycle 23 (1995–2005) data on which it was developed, the method has a probability of detection of 63% (47/75), a false alarm rate of 42% (34/81), and a median warning time of ~55 min for the 19 events successfully predicted by our technique for which SEP event onset times were provided by Posner (2007). These measures meet or exceed verification results for competing automated SEP warning techniques but, at the present stage of space weather forecasting, fall well short of those achieved with a human (aided by techniques such as ours) making the ultimate yes/no SEP event prediction. We give some suggestions as to how our method could be improved and provide our flare and SEP event database in the auxiliary material to facilitate quantitative comparisons with techniques developed in the future.

Citation: Laurenza, M., E. W. Cliver, J. Hewitt, M. Storini, A. G. Ling, C. C. Balch, and M. L. Kaiser (2009), A technique for short-term warning of solar energetic particle events based on flare location, flare size, and evidence of particle escape, *Space Weather*, *7*, S04008, doi:10.1029/2007SW000379.

1. Introduction

1.1. Motivation

[2] Solar energetic proton (SEP) events constitute a hazardous condition in interplanetary and near-Earth space. SEPs damage electronic components on satellites and produce spurious signals which can lead to spacecraft malfunction [*Feynman and Gabriel*, 2000; *Dyer et al.*, 2004; *Iucci et al.*, 2005]. SEPs also pose a radiation threat for astronauts [*Cucinotta et al.*, 2002; *Hoff et al.*, 2004] and crews of high-flying aircraft and commercial airlines in polar routes [*Beck et al.*, 2005; *Dyer et al.*, 2005, *Getley et al.*, 2005]. Finally, SEPs can impact the polar ionosphere, causing absorption of high-frequency radio waves, thereby affecting long-distance radio communication and radar systems [*Hunsucker*, 1992; *Hargreaves*, 2005]. Hence, a warning system is required in order to predict SEP event occurrence and mitigate their impacts.

1.2. SEP Event Forecasting: State of the Art

[3] Current methods for forecasting SEPs rely on observations of associated solar phenomena and the difference between the transit time of electromagnetic signatures of SEP acceleration/escape and the time required for a >10 MeV proton event to meet/exceed the NOAA Space Weather Prediction Center (SWPC) SEP threshold of J (>0 MeV) = 10 proton flux units (1 pfu = 1 pr cm^{-2} sr^{-1} s^{-1}). In an alternative approach, *Posner* [2007] recently developed an electron-based prediction technique that exploits the shorter transit time of electrons relative to ions. At present, the principal acceleration mechanism for >10 MeV protons is under debate, with advocates divided between CME-driven shocks [*Reames*, 1999a; *Cliver et al.*, 2004; *Tylka et al.*,

[1]Institute of Interplanetary Space Physics, INAF, Rome, Italy.
[2]Space Vehicles Directorate, AFRL, Hanscom Air Force Base, Massachusetts, USA.
[3]Atmospheric Environmental Research, Inc., Lexington, Massachusetts, USA.
[4]NOAA Space Weather Prediction Center, Boulder, Colorado, USA.
[5]NASA Goddard Space Flight Center, Greenbelt, Maryland, USA.

2005] and a post-CME (flare) reconnection process [e.g., *Cane et al.*, 2002; *Klein et al.*, 2005; *Marque et al.*, 2006]. Physics-based numerical models of SEP acceleration at shocks [e.g., *Roussev et al.*, 2004; *Zank et al.*, 2005; *Sokolov et al.*, 2006] have not yet reached the point where they can be used in an operational setting. No research to date has combined accurate simulations of shock evolution, particle injection and acceleration and interplanetary transport [see *Lario*, 2005]. The post-CME reconnection process for SEP acceleration also lacks an operational model.

[4] The present SEP prediction model used in operations at NOAA SWPC is called "Protons" [*Balch*, 1999]. This model, first implemented in real time during the declining years of solar cycle 20 [*Heckman*, 1979], is based on the standard assumption that there is a relationship between the intensity of solar flare emissions and SEP event occurrence. It estimates the probability (P) for the occurrence of a SEP event following a soft X-ray (SXR; 1–8 Å) burst based on the SXR peak flux and time-integrated flux, the occurrence or nonoccurrence of type II and/or type IV radio bursts, and the Hα flare location. Protons was recently validated by *Balch* [2008] who found that for the period from 1986 to 2004, the probability of detection (POD) of SEP events meeting the NOAA SWPC SEP event threshold was 57% with a false alarm rate (FAR) of 55%.

[5] At SWPC, the Protons program is only used as a decision aid, however, and the final yes/no SEP prediction is made by a forecaster. Thus the SEP event forecasts issued by SWPC are significantly more accurate than those given by Protons alone, and, moreover, have been improving with time (http://www.swpc.noaa.gov/forecast_verification/ProtonWarning.html). For the interval from 1995 to 2005 on which the study presented herein is based, the SWPC SEP POD was 88% (78/89) with a FAR of 18% (17/95). The challenge for the solar-terrestrial community is to develop automated/objective computer models of equivalent accuracy to those obtained with forecaster input. As has been the case for terrestrial weather forecasting, the approach to this goal will be incremental [*Siscoe*, 2006]. The present work is a step along that path.

1.3. Approach

1.3.1. Guidelines

[6] In developing a short-term warning system for SEP events, we have followed two guiding principles:

[7] 1. Maximize warning time. Thus, for model input, we have used data that are (or can be made) available to SWPC in real time. Our focus is on parameters that are observable (or can be inferred) early in an event, close to flare maximum. While this does not preclude using parameters such as CME speed, for example, it does make it imperative that such speeds be obtained/inferred very early in an event. As we will show, even with this emphasis on maximizing warning time, the median lead time for the successful (post hoc) forecasts based on our technique is only 55 min.

[8] 2. Follow an empirical approach. Basically, we rely on the "big flare syndrome" [*Kahler*, 1982], notion that big flares have more of everything. The larger the flare, the more likely it will be followed by a significant SEP event at 1 AU. The pitfalls of this flare-size-based approach, specifically the occasional occurrence of SWPC level events following eruptions with weak flare emissions (~15% (12/78) of SWPC SEP events from visible disk sources during the 1995–2005 originated in eruptions for which the associated SXR burst was <M2), have been documented by *Cliver et al.* [1983] and *Cliver* [2006]. In keeping with our use of an empirical approach, we have used a number of free parameters (as noted below) arrived at by trial and error to maximize the forecast results.

[9] Our method only indicates whether a solar eruption will produce an SWPC SEP event; it does not give an estimate of the peak proton intensity or proton fluence. Such estimates, as well as predictions of additional SEP parameters such as event peak time are provided by the Protons model [*Balch*, 1999, 2008] and the Proton Prediction Study (PPS) [*Smart and Shea*, 1979, 1989, 1992; cf., *Kahler et al.*, 2007], albeit with substantial uncertainty/inaccuracy [*Balch*, 1999].

1.3.2. Inputs to Forecast Model

[10] Our empirical SEP forecast technique is based on: flare location, flare size, and evidence of particle acceleration/escape.

1.3.2.1. Flare Location

[11] It has long been recognized that flare longitude is a critical parameter for a solar eruption to be followed by a SEP event at Earth [*McCracken*, 1962; *Van Hollebeke et al.*, 1975; *Cane et al.*, 1988; *Shea and Smart*, 1990; *Belov et al.*, 2005; *Laurenza et al.*, 2007]. Flares located near the foot point of the spiral magnetic field line from Sun to Earth (~W55° heliolongitude) are more likely to be followed by significant SEP events at 1 AU than those at eastern longitudes.

1.3.2.2. Flare Size

[12] Over 40 years ago, *Webber* [1963] presented evidence for a power law relationship between time-integrated radio flux from flares and the time-integrated SEP flux associated with the flare. Since then, there have been numerous additional studies linking various aspects of flare size to SEP occurrence [e.g., *Castelli et al.*, 1967; *Croom*, 1971a; *Sarris and Shawhan*, 1973; *Kahler*, 1982; *Nonnast et al.*, 1982; *Belov et al.*, 2005]. Our forecast scheme uses SXR integrated flare intensity as a measure of flare size because the GOES SXR data are available at SWPC in real time. In our technique, SEP event forecasts are only made for ≥M2 class 1–8 Å flares. While ~15% of the SWPC SEP events in our sample were associated with <M2 SXR flares, the probability of a well-connected <M2 SXR flare being associated with such a SEP event is very small (<10% for even M1.0–1.9 events [*Belov et al.*, 2005]). Thus, because our method is based on SXR intensity, successful prediction of SWPC level SEP events associated with <M2 class

flares (increasing the probability of detection) would be accompanied by an unacceptably high false alarm rate.

1.3.2.3. SEP Acceleration and Escape

[13] Low-frequency ($\leq$1 MHz) type III radio bursts observed from space are timely/reliable indicators that particles have been accelerated at the Sun and have escaped into the interplanetary medium. A frequency of 1 MHz corresponds to a radial distance from Sun center of $\sim$7 R_S [*Leblanc et al.*, 1998]. Thus these low-frequency bursts would seem essential ingredients of any SEP event warning scheme. *Cane et al.* [2002] reported that such events were the outstanding feature in low-frequency radio spectra in essentially all >20 MeV SEP events [see also *MacDowall et al.*, 2003]. Setting aside the ongoing debate about the origin of the type-III-producing electrons in eruptions associated with large SEP events and the proton acceleration mechanism in such SEP events [*Cane et al.*, 2002; *Cliver et al.*, 2004; *Marque et al.*, 2006; *Cliver and Ling*, 2007], we will use Wind/WAVES [*Bougeret et al.*, 1995] $\sim$1 MHz time-integrated intensities in our SEP event warning method as an indicator of SEP acceleration/escape. Low-frequency radio data from STEREO are currently available in near-real time at SWPC via the World Wide Web (http://www.stereo.gsfc.nasa.gov; data latency of 5 min although this will increase as STEREO moves further from Earth) with $\sim$70% data coverage (potential to 100%).

1.4. Roadmap

[14] In section 2, we present and discuss the flare and SEP databases for the solar cycle 23 interval used in this study. In section 3, we present and evaluate our technique and in section 4 we summarize and discuss our results.

2. Database

2.1. SEP List

[15] We compiled a list of SEP events for solar cycle 23 (January 1995 to December 2005) from the 5-min proton data measured on board the GOES satellite series (available at http://spidr.ngdc.noaa.gov/spidr/index.jsp). We required a >10 MeV proton flux $\geq$10 pfu for three consecutive 5-min intervals to define a proton enhancement as a SEP event. (When a SEP event was observed by more than one GOES spacecraft, we used the data from the satellite which recorded the largest event peak intensity. For the large majority of events, intensity differences between spacecraft are small.) The threshold of 10 pfu is approximately 2 orders of magnitude above the normal background and represents the lowest intensity where radiation hazard analysis is needed. We did not consider solar particle enhancements which did not meet this threshold in our analysis, e.g., a forecast of a SEP event by our technique followed by a >10 MeV event with peak intensity of 9 pfu was considered to be a false alarm. For times when the >10 MeV proton background was $\geq$10 pfu, we required an increase by a factor of two to register a new SEP event.

[16] We associated each identified SEP event with a solar source, either (1) a visible disk flare or disappearing filament or (2) a partially observed, or inferred, behind-the-limb eruption. In making flare associations, we aimed to separate the proton enhancements from different solar flares to the best of our ability. We attributed each SEP increase above the SWPC threshold (or each increase of a factor of two above a $\geq$10 pfu background) to a single solar event. For example if two flares, A and B, were followed by an increase to 7 pfu and a second increase (from 7 pfu) to 12 pfu, we would assign the SWPC SEP event to flare B. This is a necessary simplification for a prediction scheme because a yes/no SEP event occurrence decision must be made on every SXR flare which exceeds the threshold (M2 in our case) for making a forecast.

[17] From 1995 to 2005, we identified 93 prompt SEP events meeting the NOAA criteria for a significant event. Our definition of "prompt" includes SEP events for which the onset (e.g., 15 July 2002) and/or the peak (e.g., 17 November 2001) may have been delayed from the flare because of propagation effects (e.g., 15 March 2002) as long as it appeared that the rise exceeded the $\geq$10 pfu threshold outside the time of any shock spike. We did not include six SEP events which only met the SWPC threshold as a result of shock spikes (associated with solar eruptions on 23 September 1998, 20 January 1999, 3 May 1999, 9 August 2000, 26 April 2001, and 12 September 2004). Similarly we did not consider shock spikes, as well as modulations caused by nonshock solar wind structures, associated with a prompt event on our list (e.g., solar events on 26 December 2001, 18 March 2002, and 7 November 2004). Advance warning for such shock spikes or energetic storm particle (the so-called ESP) events, which can have very intense >10 MeV peaks [*Reames*, 1999b], may be provided by shock/SEP monitoring from L1 [*Cohen et al.*, 2001].

[18] Attribution of SEP events to solar sources was a critical part of our study. For most of these large (J (>10 MeV) $\geq$ 10 pfu) SEP events, the process is straightforward but difficulties do arise for behind-the-limb sources as well as for events for which the Sun was poorly observed. Generally, we identified the largest soft X-ray flare near the SEP event start time as the SEP source, taking into consideration time coincidence with type II and IV events and fast CMEs (all in accordance with the big flare syndrome, as well as the current CME-driven shock picture of large SEP events). Despite our use of the various mentioned observables (e.g., type IIs, IVs, and CMEs) in associating the SEP events in Table 1 with solar eruptions, our warning technique relies only on the parameters (flare location, size, and evidence for particle acceleration/escape) specified in section 1.3.2. Active region histories were an important factor in attributing SEP events to solar backside sources; coronagraph, extreme ultraviolet (EUV) and soft X-ray images in the LASCO CME catalog (http://cdaw.gsfc.nasa.gov/CME_list/) were also particularly helpful for identifying backside sources. To obtain our final list of SEP events, we made two independent determinations of SEP events and their

Table 1. SEP Flare List[a]

Event Number	SXR Date	Peak Time	SXR Class	Hα Location	SXR Fluence Used (J/m^2)	SXR Flag	Wind/Waves Fluence (sfu × min)	Frequency (kHz)	Delay to Onset[b] (min)	SEP Forecast Result
1	20 Oct. 1995	0606	M1.7	S11W53	3.28E−2	5	5.99E+5	940		MISS
2	4 Nov. 1997	0558	X2.1	S15W34	5.86E−2	7	1.20E+7	940	36	Hit
3	6 Nov. 1997	1155	X9.4	S18W63	3.61E−1	7	1.87E+7	940	61	Hit
4	20 Apr. 1998	1021	M1.5	W115						
5	2 May 1998	1342	X1.2	S15W15	7.37E−2	5	2.14E+7	940	56	Hit
6	6 May 1998	0809	X2.8	S11W65	2.35E−1	5	8.85E+6	940	13	Hit
7	9 May 1998	0340	M7.7	W100	1.08E−1	5	2.69E+6	940		Hit
8	24 Aug. 1998	2212	X1.1	N35E09	1.88E−1	5	1.79E+7	940		Hit
9	30 Sep. 1998	1348	M3.0	N23W81	9.61E−2	2	7.09E+5	940		Hit
10	14 Nov. 1998	0518	C1.8	W130						
11	24 Apr. 1999	1300	<C1	W130						
12	1 Jun. 1999	1845	C?	>W90						
13	4 Jun. 1999	0703	M4.2	N17W69	2.62E−2	5	3.95E+6	940		Miss
14	18 Feb. 2000	0925	C?	W120						
15	4 Apr. 2000	1539	M1.0	N15W63	3.30E−2	2	9.24E+6	940		MISS
16	6 Jun. 2000	1525	X2.5	N21E15	4.22E−1	5	1.28E+7	940	205	Hit
17	10 Jun. 2000	1700	M5.6	N22W39	1.02E−1	5	9.57E+6	940	20	Hit
18	14 Jul. 2000	1023	X6.1	N22W07	1.35E+0	5	1.20E+7	940	15	Hit
19	22 Jul. 2000	1132	M3.9	N14W56	8.18E−2	5	1.69E+5	940		Miss
20	27 Jul. 2000	1930	C?	>W120						
21	12 Sep. 2000	1212	M1.0	S19W08	2.94E−2	1	5.43E+6	940		MISS
22	16 Oct. 2000	0735	M2.8	W110	8.54E−2	1	7.18E+4	940		Miss
23	25 Oct. 2000	1109	C4.1	>W90						
24	8 Nov. 2000	2327	M7.9	N10W77	3.36E−1	3	4.51E+6	940	−3	Hit
25	24 Nov. 2000	1513	X2.5	N21W08	1.64E−1	5	6.77E+6	940		Hit
26	25 Nov. 2000	0131	M8.4	N07E50	2.66E−1	5	1.69E+6	940		Miss
27	28 Jan. 2001	1558	M1.7	S04W59	3.54E−2	5	1.60E+6	940		MISS
28	29 Mar. 2001	1015	X1.8	N14W13	2.74E−1	5	3.83E+5	940		Miss
29	2 Apr. 2001	2150	X18.4S	N18W82	1.62E+0	5	2.75E+6	940		Hit
30	10 Apr. 2001	0526	X2.3	S23W09	3.66E−1	5	9.50E+6	940		Hit
31	12 Apr. 2001	1028	X2.2	S19W43	4.02E−1	5	6.54E+6	940		Hit
32	15 Apr. 2001	1350	X15.8	S20W85	6.20E−1	7	8.77E+6	940	28	Hit
33	18 Apr. 2001	0214	C2.4	W120						
34	7 May 2001	1220	C4.1	W35	1.22E−2	5	1.50E+4	940		MISS
35	15 Jun. 2001	1530	<C2	W115						
36	9 Aug. 2001	1122	C3.9	W10	1.08E−2	5	1.57E+4	940		MISS
37	15 Aug. 2001	2355	<C1	W180						
38	15 Sep. 2001	1128	M1.6	S21W49	5.35E−2	2	1.98E+4	940		MISS
39	24 Sep. 2001	1035	X2.7	S17E29	1.09E+0	3	1.48E+6	940	75	Hit
40	1 Oct. 2001	0515	M9.1	S22W85	7.56E−2	5	1.12E+5	940		Miss
41	19 Oct. 2001	1630	X1.8	N15W29	1.66E−1	5	3.38E+4	940		Miss
42	22 Oct. 2001	1508	M7.0	S17E19	1.89E−1	5	1.77E+7	940	24	Hit
43	4 Nov. 2001	1619	X1.1	N07W19	2.76E−1	2	1.36E+7	940	39	Hit
44	17 Nov. 2001	0523	M3.0	S13E42	1.34E−1	3	3.69E+6	940		Miss
45	22 Nov. 2001	2034	M4.1	S25W67	6.49E−2	5	4.74E+6	940		Hit
46	22 Nov. 2001	2327	X1.0	S15W34	4.68E−1	3	1.38E+5	940		Hit
47	26 Dec. 2001	0536	M7.6	N08W54	6.30E−1	4	1.14E+6	940	6	Hit
48	28 Dec. 2001	2042	X3.5	S26E95	2.92E+0	4	4.43E+6	940		Hit
49	8 Jan. 2002	2025	C9.6	N05W95						
50	14 Jan. 2002	0623	M4.8	W90	4.03E−1	4	9.69E+4	940	115	Hit
51	20 Feb. 2002	0612	M5.7	N12W72	1.75E−2	7	7.40E+6	940		Miss
52	15 Mar. 2002	2306	M2.3	S08W03	6.34E−2	1	2.15E+6	940		Miss
53	18 Mar. 2002	0230	M1.1	W22	1.73E−2	5	2.67E+5	940		MISS
54	22 Mar. 2002	1111	M1.8	S10W95						
55	17 Apr. 2002	0824	M2.9	S14W36	1.35E−1	3	6.93E+5	1000	86	Hit
56	21 Apr. 2002	0147	X1.7	S14W84	7.82E−1	3	4.51E+6	940	−7	Hit
57	22 May 2002	0348	C5.2	S22W53	1.82E−2	1[b]	2.02E+6	940		MISS
58	7 Jul. 2002	1143	M1.2	W115						
59	15 Jul. 2002	2008	X3.2	N19W01	1.49E−1	7	9.81E+6	940	882	Hit
60	20 Jul. 2002	2128	X3.4	E100	1.08E+0	5	3.32E+6	940		Hit
61	14 Aug. 2002	0211	M2.6	N10W54	1.06E−1	3	9.51E+5	940	9	Hit
62	22 Aug. 2002	0157	M5.9	S07W62	3.82E−2	5	1.02E+7	940		Miss
63	24 Aug. 2002	0111	X3.5	S02W81	5.75E−1	5	Cal	940		
64	5 Sep. 2002	1704	C5.2	N09E28	2.49E−2	3	2.34E+5	940		MISS
65	9 Nov. 2002	1323	M4.9	S12W29	5.52E−2	5	8.14E+6	940	55	Hit
66	28 May 2003	0027	X3.9	S07W21	3.12E−1	5	7.20E+6	940		Hit

Table 1. (continued)

Event Number	SXR Date	Peak Time	SXR Class	Ho Location	SXR Fluence Used (J/m^2)	SXR Flag	Wind/Waves Fluence (sfu × min)	Frequency (kHz)	Delay to Onset[b] (min)	SEP Forecast Result
67	31 May 2003	0224	X1.0	S07W65	1.20E−1	5	7.96E+6	940		Hit
68	17 Jun. 2003	2245	M6.8	S08E61	Gap	7	8.56E+4	940		
69	26 Oct. 2003	1811	X1.4	N02W38	3.83E−1	1	1.43E+6	916		Hit
70	28 Oct. 2003	1110	X18.4S	S16E07	1.96E+0	5	2.16E+7	916		Hit
71	29 Oct. 2003	2049	X10.8	S15W02	9.80E−1	5	8.79E+6	916		Hit
72	2 Nov. 2003	1725	X9.3	S14W56	1.09E+0	5	2.70E+6	916		Hit
73	4 Nov. 2003	1944	X18.4S	S19W83	2.65E+0	1	9.53E+5	916		Hit
74	20 Nov. 2003	2353	M6.2	N02W17	2.82E−2	7	7.07E+6	916		Miss
75	2 Dec. 2003	1150	C8.5	S17W95						
76	11 Apr. 2004	0419	M1.0	S14W47	1.72E−2	5	3.03E+6	940		MISS
77	25 Jul. 2004	1515	M1.2	N08W33	3.25E−2	1	7.51E+4	940		MISS
78	19 Sep. 2004	1711	M2.0	N05W58	5.46E−2	5	4.20E+6	940		Hit
79	1 Nov. 2004	0555	<C1	>W90						
80	7 Nov. 2004	1606	X2.2	N09W17	2.08E−1	5	1.36E+6	940		Hit
81	10 Nov. 2004	0213	X2.8	N09W49	1.68E−1	7	1.84E+6	940		Hit
82	15 Jan. 2005	2300	X2.9	N14W08	8.63E−1	2	1.01E+6	916		Hit
83	17 Jan. 2005	0952	X4.2	N14W24	7.20E−1	5	1.63E+6	916		Hit
84	20 Jan. 2005	0700	X7.9	N12W58	1.97E+0	5	1.66E+7	916		Hit
85	13 May 2005	1657	M8.5	N12E11	2.50E−1	5	1.79E+7	916		Hit
86	16 Jun. 2005	2022	M4.3	N09W87	7.75E−2	5	6.94E+5	916		Miss
87	13 Jul. 2005	1449	M5.6	N13W75	4.64E−1	4	1.08E+5	916		Hit
88	14 Jul. 2005	1054	X1.4	W95	6.63E−1	3	2.65E+4	916		Miss
89	17 Jul. 2005	1120	<1	W135						
90	27 Jul. 2005	0501	M3.8	<E90	1.16E−1	5	8.83E+4	916		Miss
91	22 Aug. 2005	1728	M6.2	S12W60	2.87E−1	3	1.54E+6	916		Hit
92	7 Sep. 2005	1740	X18.1	S06E89	6.65E+0	3	1.42E+7	916		Hit
93	13 Sep. 2005	2004	X1.6	S09E05	4.86E−1	5	1.49E+5	916		Miss

[a]Here J (>10 MeV) ≥ 10 pfu.

[b]Values based on published SEP onset times are by *Posner* [2007]. The listed time does not include the time required for the event to rise above the SWPC ≥ 10 pfu prediction threshold nor the 15 min required to certify a new SEP event.

solar associations (one by Laurenza, Cliver, and Hewitt and one by Balch) and reconciled discrepancies, also taking into account a third list of SEP events (based on the NOAA list at http://umbra.nascom.nasa.gov/SEP/) with associations independently determined by *Cane et al.* [2006].

[19] Our final reconciled list of SEP events with their solar associations is reported in Table 1. The information in the Table 1 is as follows: (1) event number; (2) event date (of the associated solar event); (3) peak time of soft X-ray burst (when the SXR class is indefinite, this time refers to the onset of the 1MHz emission; no SXR integration was attempted for these events); (4) soft X-ray burst class (saturated events flagged with an "S" in which case (3) refers to the onset of saturation); (5) heliographic location of associated solar eruption (from *National Geophysical Data Center* [2006] or determined from SXR and/or EUV images in the LASCO CME catalog); (6) time-integrated SXR intensity (nominally (see section 3.1.2) taken between the 1/3 power points on the rise and decay of the event; no SXR integration was made for <M2.0 events from beyond the limb); (7) SXR integration flag (defined in section 3.1.2); (8) time-integrated 1 MHz Wind/WAVES type III intensity from 10 min before the onset of SXR event to 10 min after the SXR burst peak; (9) Waves frequency used; (10) delay time from SXR peak +10 min (time of forecast) to the >30 MeV SEP event onset (taken from *Posner* [2007]); and (11) SEP Forecast Result ("Hit", SEP event correctly predicted; "Miss", SEP event from frontside or backside source with peak intensity ≥M2 not predicted; no entry indicates either that the responsible eruption was located on the backside of the Sun and the associated SXR flare was <M2 (16 cases) or that SXR or radio data were unavailable (2 cases)). Note that while no prediction was made for SEP events associated with visible disk eruptions for which the associated SXR flare was <M2, such events were assigned to the Miss class (given as "MISS" in Table 1 to distinguish them from the normal Miss events associated with ≥M2 flares) because, unlike the small (<M2) behind-the-limb flares, the model inputs in these cases were not compromised. SEP events associated with small (<M2) behind-the-limb (>90° longitude) flares are not counted as misses because the required input data, as the accurate measurement of the integrated SXR intensity, is not available because of likely limb occultation. Thus it seems fair to not count these events as misses in much the same sense that we exclude events with data gaps. At the same time, we issued a hypothetical forecast for every ≥M2 SXR flare, regardless of flare location. It may be possible (and is certainly desirable) to improve forecasts of SEP events from behind the limb sources by, e.g., using STEREO type observations that look beyond the limb or with a particle-based technique such as that of *Posner* [2007], but such an extension is beyond the scope of the present paper.

[20] Figure 1 gives the longitudinal distribution of the 93 prompt SEP events (using the best guess longitude for

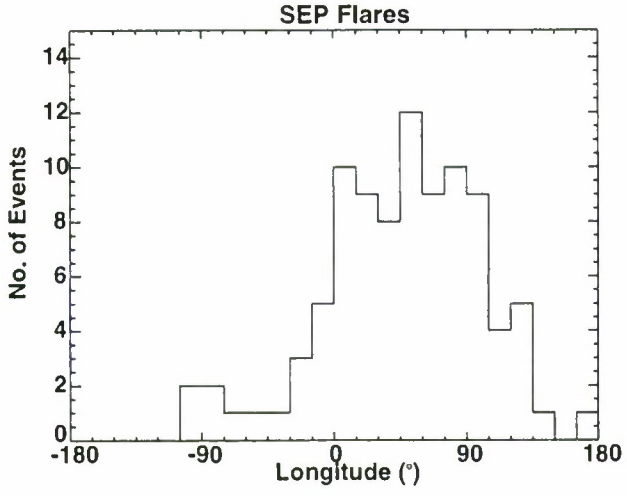

Figure 1. Flare heliolongitudes (in 15°) bins for the 93 SWPC prompt SEP events during cycle 23 (1995–2005).

SEP events originating on the backside of the Sun). The familiar western bias of such events is apparent.

2.2. Soft X-Ray List

[21] From 1995 to 2005, we identified 704 ≥M2 SXR flares in the GOES 1-min averaged 1–8 Å data (available at http://spidr.ngdc.noaa.gov/spidr/index.jsp). In making the flare associations for the ≥M2 soft X-ray events, we used the list of Hα flares from *National Geophysical Data Center* [2006] in conjunction with the daily soft X-ray plots. For events with no reported Hα flare, we made associations using the EIT and SXT data from the SOHO LASCO CME catalog as well as active region histories and the narrative texts in The Weekly: Preliminary Report and Forecast of Solar Geophysical Data (Space Weather Prediction Center, available at http://www.sec.noaa.gov/weekly/index.html; for these events only longitudes are listed in the flare location). The Boulder reports were particularly helpful in the sense that they often indicated sources of SXR flares that lacked an Hα counterpart, giving the forecaster's best guess based on the data available at the time and thus injecting realism into the exercise, since these educated guesses would be folded into our technique evaluation. As was done for the SEP events in Table 1, the list of X-ray events and associations was compiled separately by two subgroups of coauthors (Laurenza, Cliver, and Hewitt and Balch (1995–2004)) and then reconciled. Because we used the largest peak SXR intensity observed by any GOES satellite, our list includes 55 more events (all with intensity classes ≤M2.6; 51 ≤M2.2) than that compiled by *Balch* [2008] for the 1995–2004 period of overlap.

[22] The list of 704 SXR flares is given in Data Set S1 in the auxiliary material.[1] The information in Data Set S1 is as follows: (1) event number; (2) date of the SXR flare; (3) peak time of SXR flare; (4) peak SXR classification (saturated events flagged with an S in which case (3) refers to the onset of saturation); (5) flare location; (6) time-integrated SXR intensity (nominally between the 1/3 power points on rise and fall (see section 3.1.2)); (7) ratio of the SXR intensity at the peak time +10 min (I_{10}) to the SXR intensity at the event peak (I_P) (see section 3.1.2); (8) extrapolated/adjusted time-integrated SXR intensity (see section 3.1.2); (9) SXR integration flag (defined in section 3.1.2); (10) ratio of (8) to (6); (11) time-integrated SXR intensity used in analysis (taken from either (6) or (8)); (12) time-integrated 1 MHz Wind/WAVES intensity from 10 min before the onset of integration for the SXR burst to 10 min after the SXR burst peak; (13) waves frequency used; and (14) SEP forecast result (Hit, SEP event correctly predicted; Miss, SEP event from frontside or backside source with peak intensity ≥M2 not predicted; "False Alarm", SEP event predicted but none occurred; "Correct Null", i.e., no SEP event predicted and none occurred); a blank indicates a gap either in the SXR or radio data or that the radio burst occurred during calibration.

[23] Figure 2 gives the longitude distribution, binned by 15°, of all the ≥M2 flares in Data Set S1. Note that, in comparison with the longitudinal distribution of all Hα flares [*Wright*, 1980], the distribution in Figure 2 is relatively flat across the solar disk. This reflects both the large size of ≥M2 SXR bursts, facilitating observation of their Hα counterparts for foreshortened near-limb events, and the use of imaging data from Yohkoh SXT and SOHO EIT to augment the Hα data.

3. Analysis

3.1. Input Parameters

[24] As noted in section 1.3.2, we used the following three parameters as input in our forecast scheme: (1) flare

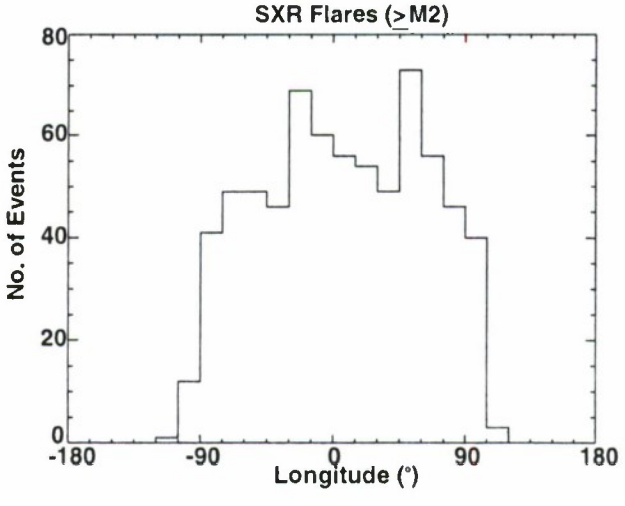

Figure 2. Flare heliolongitudes (in 15°) bins for the 704 ≥M2 SXR flares events during cycle 23 (1995–2005).

[1]Auxiliary material data sets are available at ftp://ftp.agu.org/apend/sw/2007SW000379. Other auxiliary materials files are in the HTML.

longitude; (2) time-integrated SXR intensity; and (3) time-integrated ~1 MHZ radio intensity.

3.1.1. Flare Longitude

[25] Comparison of Figures 1 and 2 reveals the much lower probability of SWPC SEP events arising in eastern versus western hemisphere activity. For the 1995–2005 interval, 15 SEP events and 327 ≥ M2 flares originated in the eastern solar hemisphere giving a 5% (15/327) SEP event "yield"; in the western hemisphere the corresponding percentage is 21% (78/377). Hence, in our forecast technique, we consider three heliolongitude ranges (E120°–E41°, E40°–W19°; W20°–W120°) separately, with the number and ranges of these longitude bins determined by trial and error in order to optimize the prediction results.

3.1.2. Time-Integrated Soft X-Ray Intensity

[26] It is well established [*Croom*, 1971b; *Nonnast et al.*, 1982; *Kocharov et al.*, 1983; *Cane et al.*, 1986] that large SEP events are preferentially (although not exclusively [e.g., *Kahler et al.*, 1991]) associated with flares with long time scales. Because of the need to maximize warning time for a SEP event, however, it is not practicable to integrate over the full duration of such flares, which can last for hours. To obtain a representative measure of the full integrated intensity, we decided to integrate (after a trial and error process) between the 1/3 power points on the rise and fall of the SXR burst. In 33% (229) of the 704 cases in Data Set S1, the SXR intensity fell to 1/3 of its maximum value within 10 min of the time of flare maximum (these events are indicated by a blank in extrapolated SXR entries and a "7" in SXR flag entries of Data Set S1). For the remaining 67% of the bursts, the time to drop to this level exceeded 10 min. For these cases (indicated by values of 1–6 in SXR flag entries of Data Set S1), we fit an exponential curve over the five 1-min data points spanning minutes 6 through 10 following the burst maximum and extrapolated this curve to the 1/3 power point to obtain the SXR integrated intensity used in our analysis. If a complete or significant data gap occurred during the time of interest in a given event, the SXR fluence is given as "Gap" in Table 1 and Data Set S1.

[27] Our SXR flux integration technique for events that did not fall to the 1/3 power point within 10 min requires two footnotes. First, saturation can produce flat traces for the interval from 6 to 10 min after burst peak while blended peaks can result in rising profile (yielding I_{10}/I_P ratio +1 and >1, respectively). For these special cases (15 in all) we assigned, after a process of trial and error, a decay slope (coefficient in the exponent) that produced a 25% drop from the measured SXR peak intensity after 10 min. Second, inspection showed that events with a high (>0.85) ratio of the (fitted) SXR intensity at the peak time +10 min (I_{10}) to the (fitted) SXR intensity at the time of the event peak (I_P) (this ratio is given by the extrapolated SXR of Data Set S1) tended to have time-integrated intensities that were overestimates. To adjust for this effect, we applied the following prescription (again arrived at by trial and error): (1) if $0.85 < I_{10}/I_P \leq 0.90$, then $I_{10}/I_P = 0.85$; (2) if $0.90 < I_{10}/I_P \leq 0.95$, then $I_{10}/I_P = 0.90$; and (3) if $0.95 < I_{10}/I_P < 1.0$, then $I_{10}/I_P = 0.95$. No adjustments were made for $I_{10}/I_P \leq 0.85$. When calculating the SXR fluence of events for which extrapolation was required, we began the (forward) integration in all cases from the peak time of the event. If no adjustment was required (i.e., $I_{10}/I_P \leq 0.85$), we integrated under the actual data points until the peak time +10 min and under the fitted line thereafter. For events requiring adjustment, we integrated under an extrapolated curve with prescribed slope starting from the measured peak time and intensity of the event and ending when the fitted intensity dropped below 1/3 of the peak intensity.

[28] For all the SXR events in Data Set S1, we made a determination of the actual integrated flux between the 1/3 power points, in order to assess the reliability of our extrapolation/adjustment technique. This integration can be problematic for (1) small (i.e., ~M2) bursts on an elevated background, (2) "blended" SXR flares which appear as long decay events, and (3) a few genuine slow rise and fall events. For such events, with unusually long (artificial or natural) rise or decay times, we arbitrarily began the integration 60 min before the burst peak (21 cases) and/or ended it within 300 min after the burst peak (1 case). The effect of the extrapolations and adjustments can be seen in Figure 3, which contains a scatterplot of the ratio of the SXR fluence used in the analysis to the measured time-integrated SXR intensity between the 1/3 power points (used fluence/measured fluence in Data Set S1) versus I_{10}/I_P (extrapolated SXR in Data Set S1) before (top) and after (bottom) the adjustments for positive slopes and high I_{10}/I_P ratios were applied. It can be seen that the various adjustments applied move the ratio of used to measured fluence closer to one for high I_{10}/I_P ratios, as desired. In all, 33 events lie more than a factor of two away from a ratio of one, i.e., with values ≤0.5 or ≥2.0. In general, events with low values of the extrapolated (adjusted)/measured SXR fluence (range from 0.03 to 0.48; 17 cases) are not a problem, because they indicate that the extrapolation has effectively removed the contribution from a subsequent closely spaced peak which would be evaluated separately. Events with large values of this ratio (range from 2.01 to 5.19; 16 cases) can result when a flat-topped burst drops sharply after the peak +10 min forecast time. The effect of both underestimates and overestimates of the SXR fluence (resulting from our extrapolation/adjustment technique) will be considered in section 3.4.1.

[29] To note the fact that the integrated SXR intensities for the cases described above involving extrapolation as well as ad hoc adjustments, we included a SXR integration flag in Table 1 and Data Set S1. The values of this flag, the circumstances in which it applies, the corresponding

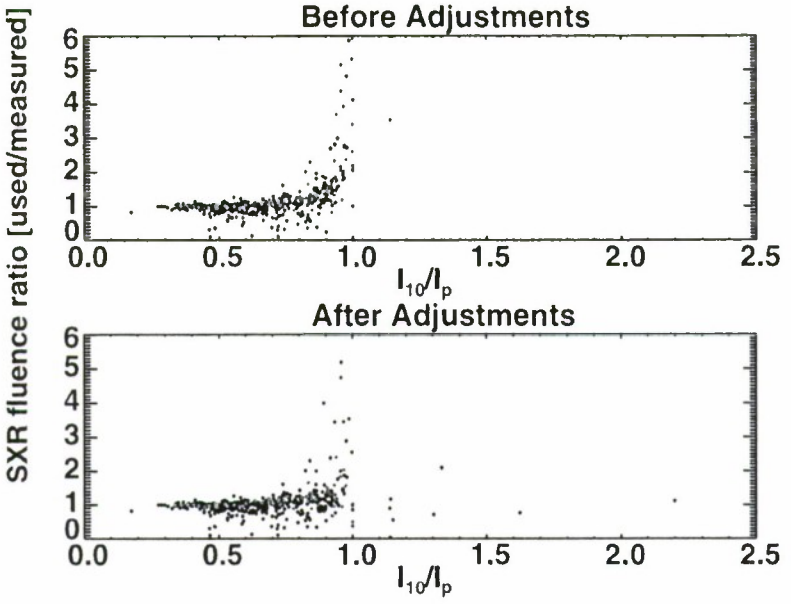

Figure 3. Scatterplot for all events in Data Set S1 of the ratio of the SXR fluence used in our analysis to the measured time-integrated SXR intensity between the 1/3 power points (used fluence/measured fluence in Data Set S1) versus I_{10}/I_P (extrapolated SXR in Data Set S1) (top) before and (bottom) after the adjustments for positive slopes and high I_{10}/I_P ratios were applied. Only points with SXR flags in Data Set S1 (SXR flag) with values from 1 to 6 are plotted. Red points indicate SEP events for which a forecast would have been made.

adjustment, and the number of cases of each type of event are given in Table 2.

3.1.3. Time-Integrated 1 MHz Radio Intensity

[30] The Wind/WAVES data were taken from the website http://lep694.gsfc.nasa.gov/waves/waves.html. The data obtained from the Wind/Waves website are provided in terms of ratio (R) of the radio flux to background with the background (B) provided in units of $\mu V/Hz^{1/2}$. The radio flux in solar flux units (1 sfu = solar flux unit = 10^{-22} W m^{-2} Hz^{-1}) is then J(sfu) = $10^{10}(R*B)^2/(Z_oA)$, where Z_o is the characteristic impedance of free space (Z_o = 377Ω), and A is the area of the RAD1 antenna (1225 m^2). For much of the 1995–2005 interval considered, 940 kHz was the closest frequency to 1 MHz at which measurements were routinely made. For a ~3 month interval at the end of 2003, however, and for all of 2005, the nearest frequency was 916 kHz. For 12 other events that were randomly distributed in time the closest usable frequency was either 1000 or 1012 kHz. For 1-min averages of data at these various frequencies near ~1 MHz, spectral differences should be small.

[31] Because the 1 MHz profiles are more highly structured and less regular than the SXR time-intensity curves, the radio time-integration was cut off strictly at 10 min after the peak of the SXR burst. After some experimentation, we opted to begin the radio integration 10 min prior to the start of the X-ray integration. The units of the radio integrated intensity are sfu minutes. If a complete or significant data gap occurred during the time of interest in a given event, the integrated radio intensity is given as Gap in Table 1 and Data Set S1. Other events occurred during routine calibration intervals, in these cases "Cal" is written in Table 1 and Data Set S1. The Gap and Cal events were not used in the analysis described in section 3.3.

3.2. Individual Event Plots

[32] Figures 4–6 contain time-intensity profiles for the 1–8 Å SXR and 1 MHz radio emissions as well as for the >10 MeV protons for three representative events in Data

Table 2. Soft X-Ray Flare Integration Flag

SXR Flag[a]	I_{10}/I_P Range	Value Assigned to I_{10}/I_P	Decay Time to $I_{10}/I_P \leq$ 0.33 (min)	Number of Cases[b]
1	$I_{10}/I_P \geq 1.0$	$I_{10}/I_P = 0.75$	38	15
2	$0.85 < I_{10}/I_P \leq 0.90$	$I_{10}/I_P = 0.85$	68	35
3	$0.90 < I_{10}/I_P \leq 0.95$	$I_{10}/I_P = 0.90$	104	33
4	$0.95 < I_{10}/I_P < 1.0$	$I_{10}/I_P = 0.95$	214	17
5	$0.33 < I_{10}/I_P \leq 0.85$	No Adjustment		367
6	$I_{10}/I_P \leq 0.33$	No Adjustment		6
7	$I_{10}(d)/I_P(d) < 0.33$	No Extrapolation		228

[a]An asterisk (plus sign) following the numerical flag in Table 1 and Data Set S1 indicates that the rise (decay) time of the SXR burst used for the integration was cut off at 60 (300) min.

[b]No SXR data for three events.

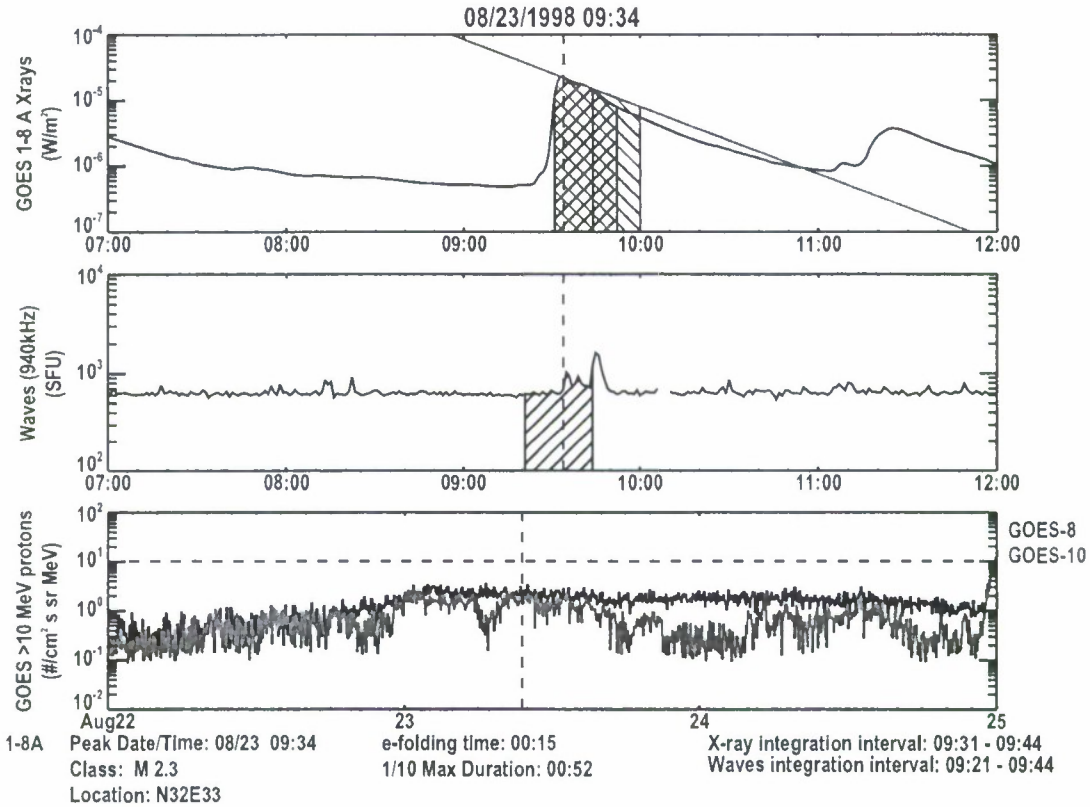

Figure 4. (top) Example of a SXR event which required no adjustment to the slope of the extrapolated exponential fit used for the soft X-ray fluence integration between the 1/3 power points. The red-hatched area indicates the SXR fluence based on the extrapolated fit to the decay of the SXR burst; the black-hatched area indicates the measured SXR fluence. (middle and bottom) The 1 MHz radio (with integration indicated by black hatching) and >10 MeV proton time-intensity profiles (showing data from all available GOES satellites), respectively.

Set S1. Figure 4 shows a SXR event which required no adjustment to the slope of the extrapolated exponential fit used for the soft X-ray integration between the 1/3 power points. Figure 5 shows an event for which $I_{10}/I_P = 0.988$ was reset to 0.95 in accordance with our prescription. Figure 6 shows a typical "slow rise" event for which the soft X-ray integration was arbitrarily initiated 60 min prior to the event, rather than at the 1/3 power point. While "well-behaved" events requiring either no extrapolation or no adjustment to an extrapolation to determine the SXR fluence accounted for 86% (602/701) of the sample, we note that the corresponding percentage for SEP associated flares was 35% (26/75), reflecting the tendency of large SEP events to be associated with long-duration flares. Plots in the format of Figures 4–6 are given in the auxiliary material for all of the 704 events in Data Set S1 (Figures S1–S352) as well as for all SWPC SEP events in Table 1 (Figures S353–S399).

3.3. Methodology

[33] The analysis technique known as logistic regression [*McCullagh and Nelder*, 1983] (first applied to SEP forecasts by *Garcia* [1994a]) can be used to obtain a continuous function for the probability of SEP event occurrence as a function of the integrated radio and X-ray flux (as computed in sections 3.1.2 and 3.1.3, respectively) for the SXR flares in our sample. This technique is appropriate for observational studies where each event is characterized by binary result (yes or no) and associated with a set of explanatory variables. In logistic regression analysis, the dependent variable y is the probability (P) that an event will occur, hence it is constrained between 0 and 1. The logistic model is written as

$$\log\left[\frac{\mathrm{Prob(SEPevent)}}{\mathrm{Prob(no\_SEPevent)}}\right] = \log\left[\frac{P}{1-P}\right] = \sum_{i=1}^{p} \beta_i x_i. \quad (1)$$

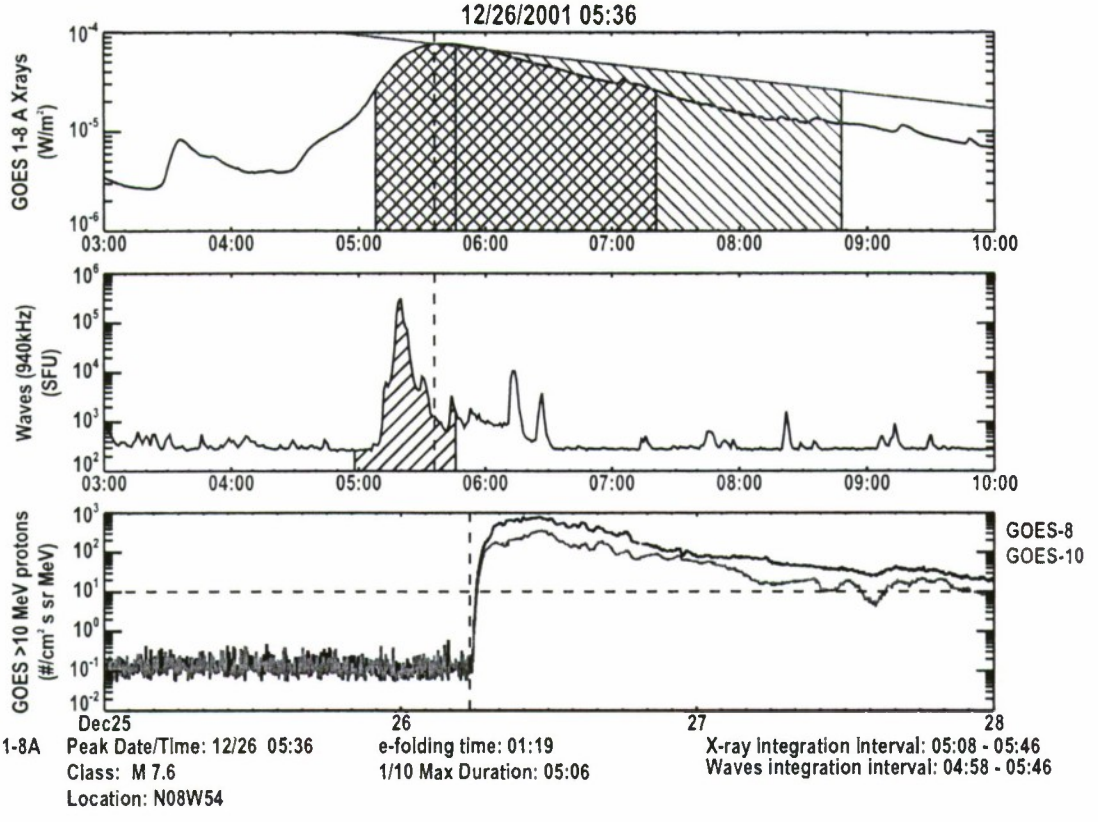

Figure 5. (top) Example of a SXR flare for which the measured I_{10}/I_P = 0.988 was reset to 0.95 in accordance with our prescription. The red-hatched area indicates the SXR fluence based on the adjusted fit to the decay of the SXR burst; the black-hatched area indicates the measured SXR fluence. (middle and bottom) The 1 MHz radio (with integration indicated by hatching) and >10 MeV proton time-intensity profiles, respectively.

where $\eta = \sum_{j=1}^{p} \beta_j x_j$ is a function of a set of environmental variables x_j through the β_j coefficients. Setting these variables to be the logarithmic value of the integrated X-ray flux X and the integrated radio flux R, the functional relationship between the probability of the event P and η becomes

$$P(\log X, \log R) = \frac{e^{\eta}}{1 + e^{\eta}}. \tag{2}$$

In this model we actually have two more terms besides the linear log X and log R components: a constant term and an interaction term between X and R. We did not include a term to take into account the dependence of SEP incidence on heliographic longitude, but we computed probability levels separately for well-connected (W20°--W120°) events as well as for two longitude ranges of increasingly poorer connection (E40°–W19° and E120°–E41°). The data, consisting of binary responses spanning the log X and log R space, yielded the following model for each of the three considered longitude intervals, respectively,

$$\begin{aligned}
\eta_1 &= -6.07 - 1.75 \log_{10}(X) + 1.14 \log_{10}(R) \\
&\quad + 0.56 \log_{10}(X) \log_{10}(R), \\
\eta_2 &= -7.44 - 2.99 \log_{10}(X) + 1.21 \log_{10}(R) \\
&\quad + 0.69 \log_{10}(X) \log_{10}(R), \\
\eta_3 &= -5.02 - 1.74 \log_{10}(X) + 0.64 \log_{10}(R) \\
&\quad + 0.40 \log_{10}(X) \log_{10}(R).
\end{aligned} \tag{3}$$

The goodness of the method was estimated by computing the standard deviation of the difference between the continuous function P(log X, log R) and the binary occurrence of SEPs in the sample considered. This estimated standard deviation is σ = 0.2. Although this is relatively high, the method yields reasonable results.

[34] The results of the model are presented in Figures 7–9 which contain scatterplots of the time-integrated 1 MHz

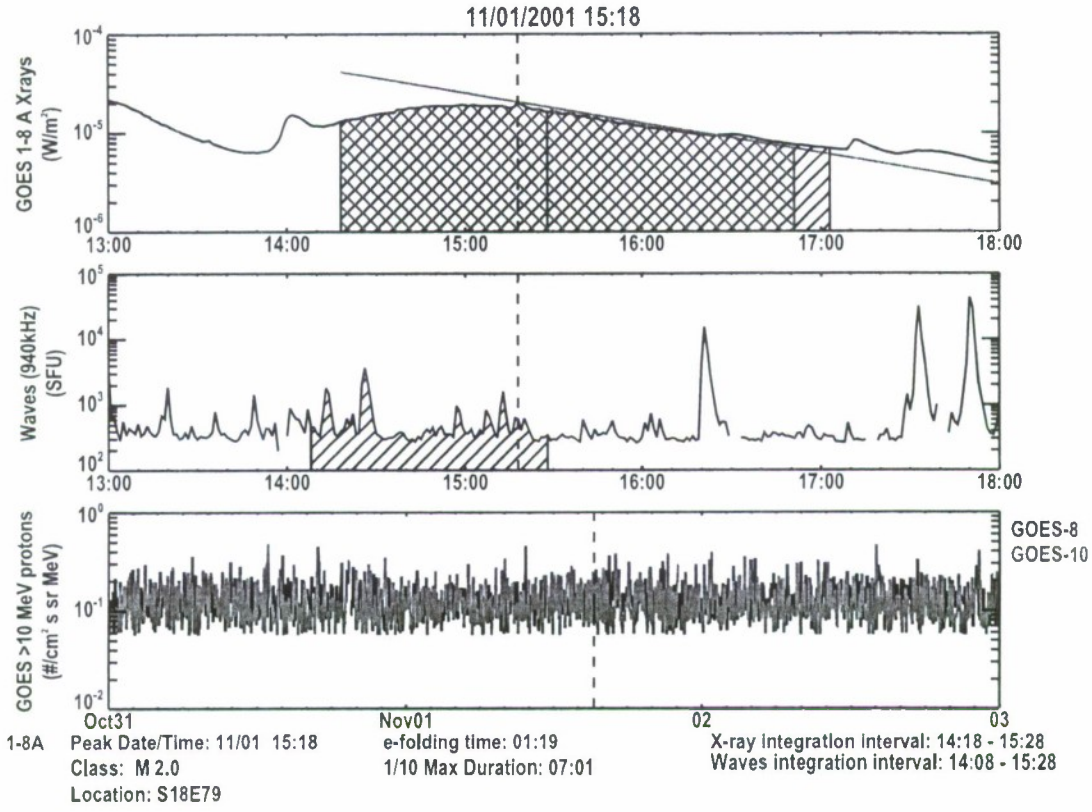

Figure 6. (top) Example of a slow rise SXR flare for which the soft X-ray integration (indicated by the hatched area) was arbitrarily initiated 1 hour prior to the event peak and for which the measured $I_{10}/I_P = 0.923$ was reset to 0.90 in accordance with our prescription. The red-hatched area indicates the SXR fluence based on the adjusted fit to the decay of the SXR burst; the black-hatched area indicates the measured SXR fluence. (middle and bottom) The 1 MHz radio (with integration indicated by hatching) and >10 MeV proton time-intensity profiles, respectively.

radio flux versus the time-integrated SXR flux, with contours for SEP event probability computed from equations (2) and (3), for events in Data Set S1 that fell in the longitude ranges of good, intermediate, and poor connection, respectively. The E40° and W20° borders between these three heliolongitude bins were determined by trial and error to optimize the forecast technique performance. For all three longitude ranges it can be seen that the probability prediction functions reflect SEP event occurrence dependence on the time-integrated X-ray and radio fluxes, although a number of SEP (non-SEP) events are located in the low- (high-) probability zone. In principle, every solar flare can be located in such diagrams, given the key parameter values, in order to evaluate the probability of a subsequent SEP event. The method allows, when choosing a specific probability contour, a yes/no binary response for the occurrence of a SEP event as follows: if flare parameters are located above the selected probability curve, a warning is issued otherwise no alert is given, as will be extensively described in the next section.

3.4. Evaluation of the Model

3.4.1. Accuracy

[35] The performance of the obtained probability forecasts can be evaluated, covering the data set on which it was developed, in terms of False Alarm Rate (FAR) and Probability of Detection (POD) as follows. Let us define a probability threshold p_t (that corresponds to selecting a contour line on plots 7–9) such that a warning will be issued whenever the forecast probability (f_p) satisfies the condition $f_p \geq p_t$ and no warning will be issued if $f_p < p_t$. Then the forecasts and observations can be compared in terms of the following variables: the number of correct forecasts or hits, A (an SWPC SEP event was forecast and one occurred); the number of false alarms, B (an SWPC SEP event was forecast but none occurred); the number of missed events, C (no SWPC SEP event was predicted but an event did occur); the number of correct nulls, D (no SWPC SEP event forecast and none occurred); the number of forecasts we would expect to be correct by chance, E; the total number of forecasts (both positive and null), N.

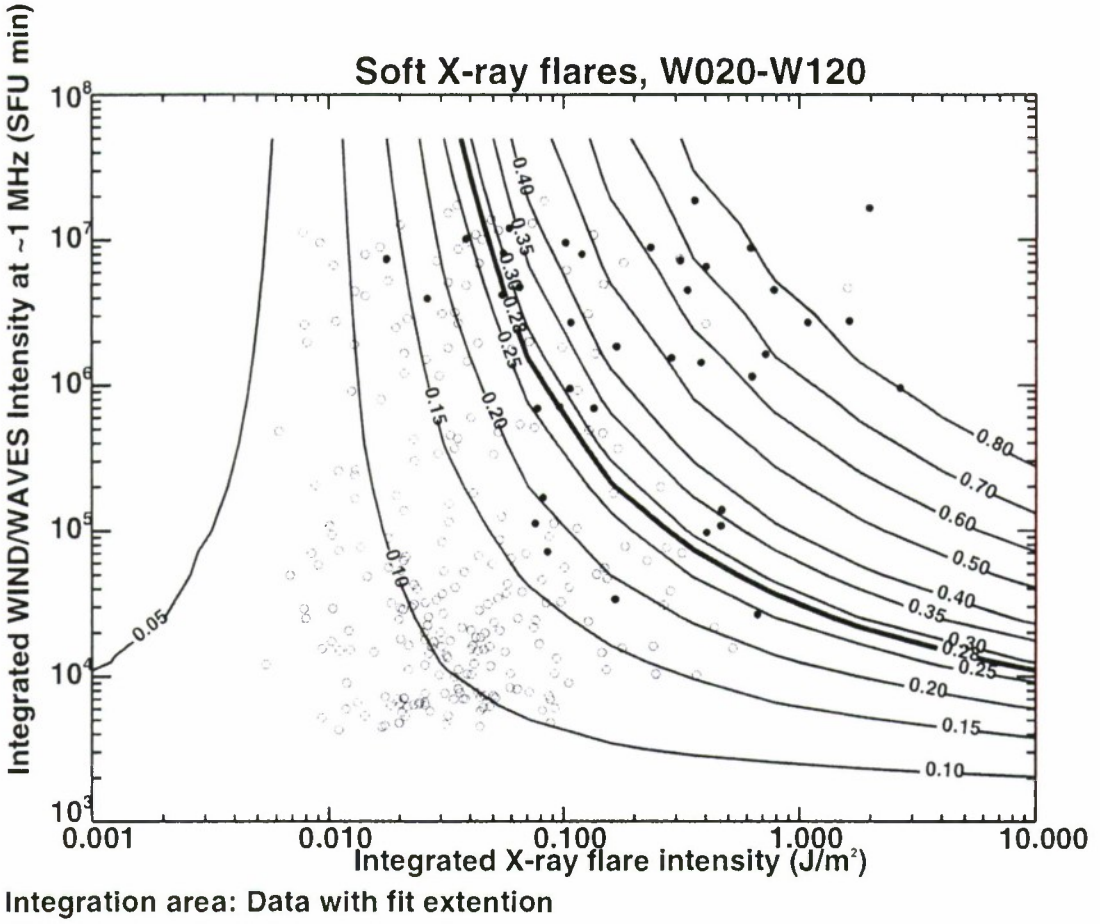

Figure 7. Integrated 1 MHz radio intensity versus integrated 1–8 Å soft X-ray intensity for ≥M2 soft X-ray flares from 1995 to 2005 located from W20°–W120°. Solid circles represent flares associated with SWPC SEP events. The black thick contour indicates the probability threshold used in the analysis.

The following statistical quantities specify the quality of these categorical forecasts: (1) probability of detection POD = A/(A + C); (2) false alarm rate FAR = B/(A + B); (3) percent correct PC = (A + D)/N; and (4) Heidke Skill Score HSS = (A + D − E)/(N − E), that is the fraction of correct forecasts adjusted by E = [(A + B)(A + C) + (B + D)(C + D)]/N [*Balch*, 2008], i.e., the number of correct forecasts by chance, that can derived according to the following argument. Given that Probability (event = Yes) = (A + C)/N and Probability (forecast = Yes) = (A + B)/N, the probability for a chance hit is the combined probability (A + C)(A + B)/N^2. Moreover, the probability of a chance correct null is the product of Probability (event = No) = (B + D)/N and Probability (forecast = No) = (C + D)/N; hence Probability (event = No and forecast = No) = (B + D)(C + D)/N^2. The combined probability for a chance correct forecast (hits and correct nulls) is [(A + C)(A + B) + (B + D)(C + D)]/N^2. We therefore derive the number of correct forecasts by chance to be E = [(A + C)(A + B) + (B + D)(C + D)]/N.

[36] For probability forecasts, the probability threshold can be treated as an independent variable ranging from 0.0 to 1.0, hence each of the categorical quality measures (POD, FAR, PC, HSS) can be considered to be a function of p_t. Figure 10 displays the categorical quality measures for the current method versus the probability threshold level: POD (thick line) and FAR (thin line) trends are shown in the Figures 10a–10c for the three considered longitude intervals; HSS (thick line) and PC (thin line) are displayed in Figures 10d–10f as well. Note that both the POD and the FAR are quite high for lower-probability thresholds and decrease with increasing threshold; HSS optimization is generally achieved for range of probabilities 20–40%. The optimal choice for p_t involves a trade off between maximizing the POD and minimizing the FAR, while achieving the HSS optimization. For the western events (Figure 10f) the optimal point is p_t = 28% (POD = 62 % (29/47), FAR = 41% (20/49), HSS = 0.53); for the "intermediate" events (Figure 10e), the optimal is reached for p_t = 28%

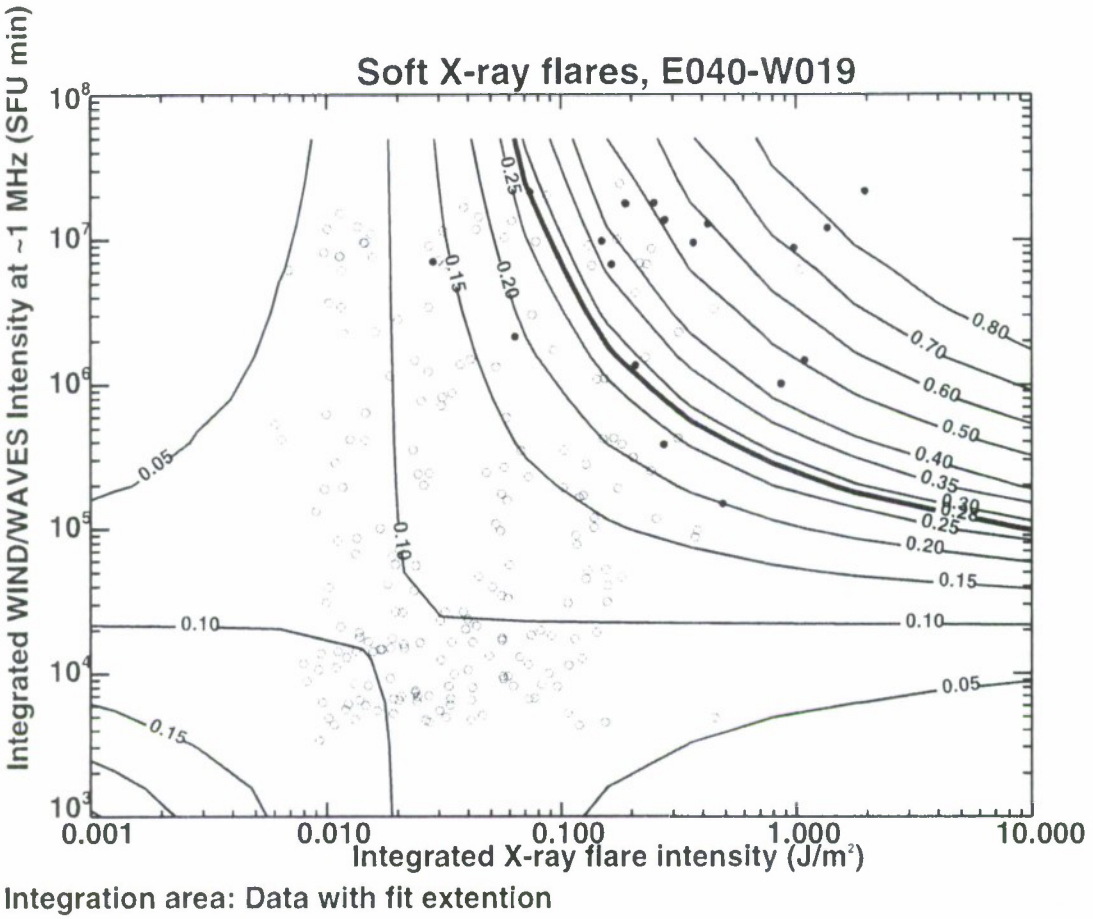

Figure 8. Integrated 1 MHz radio intensity versus integrated 1–8 Å soft X-ray intensity for ≥M2 soft X-ray flares from 1995 to 2005 located from E40°–W19°. Solid circles represent flares associated with SWPC SEP events. The black thick contour indicates the probability threshold used in the analysis.

(POD = 68% (15/22), FAR = 46% (13/28), HSS = 0.60); and for the eastern events (Figure 10d), the optimal p_t = 30% (POD = 50% (3/6), FAR = 25% (1/4), HSS = 0.59).

[37] In calculating these verification measures, we took into account that 12 SEP events were associated with disk flares of class <M2; 9 of these 12 "Misses" (since they cannot be predicted by our method) fell in the western longitude bin and 3 in the central bin. Also, we note that our extrapolations/adjustments to the SXR flux resulted in a gain of five hits (caused by events for which used fluence/measured fluence in Data Set S1 was >1.0 (Nos. 23, 435, 446, 618, 664)), a loss of one hit (used fluence/measured fluence <1.0 (No. 408)), a gain of two False Alarms (caused by events for which used fluence/measured fluence in Data Set S1 was >1.0 (Nos. 280, 484)), and a loss of two False Alarms (caused by events for which used fluence/measured fluence in Data Set S1 was <1.0 (Nos. 519, 566)). For the above cases the ratio of the used to the measured SXR fluence ranged from 0.355 to 3.53.

[38] Table 3 show the 2 × 2 contingency matrix with values of A, B, C, and D, obtained by combining events from all the heliolongitude ranges. The combined result for all longitudes is then: POD = 63% (47/75), FAR = 42% (34/81), HSS = 0.58 and PC = 93% (633/683). While this result is a clear improvement over that given by the current Protons model used at SWPC (POD = 57%, FAR = 55% [*Balch*, 1999, 2008]) and the 2-D probability models (best performer: HSS = 0.55, POD = 54%, FAR = 42% [*Balch*, 2006])), it falls well short of that obtained with forecaster input (POD = 88%; FAR = 18%).

3.4.2. Warning Time

[39] One of our guiding principles was the requirement to maximize the interval from the time that a warning is issued until the SEP event onset. Normally, the SEP onset

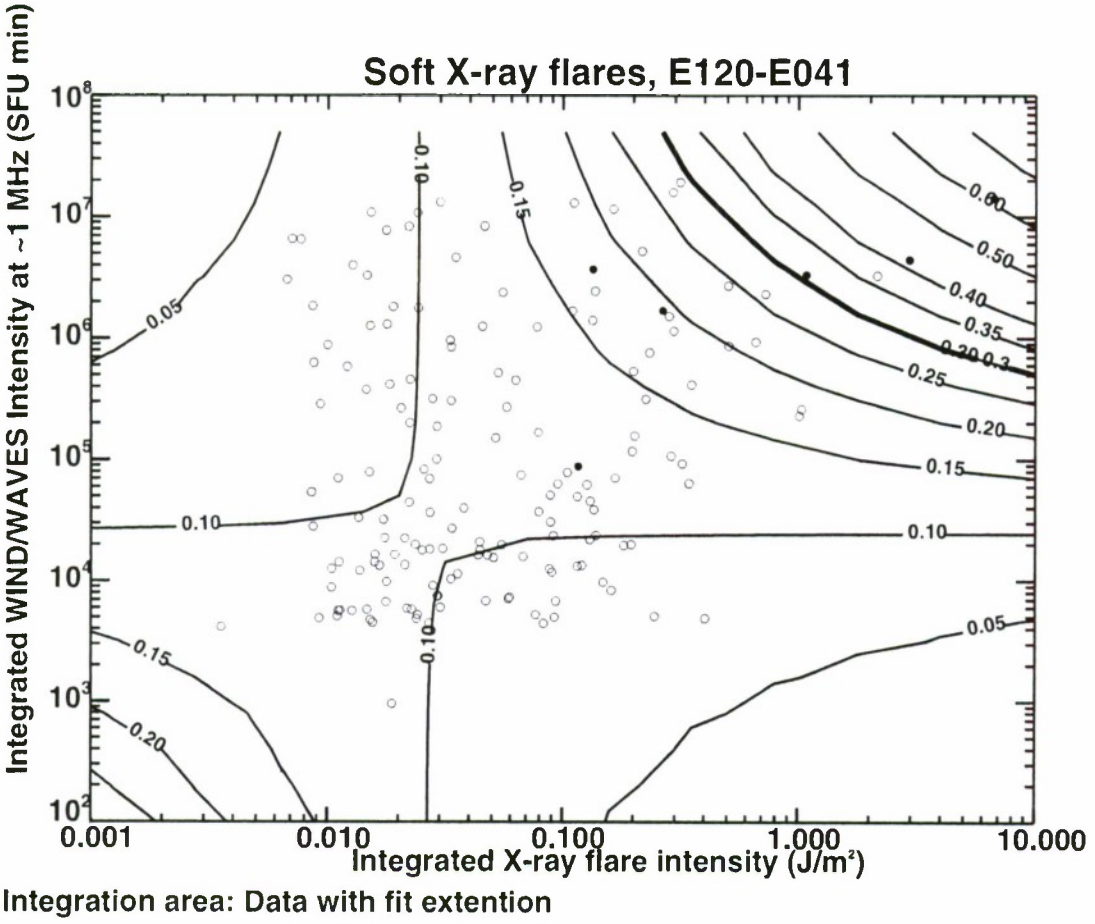

Figure 9. Integrated 1 MHz radio intensity versus integrated 1–8 Å soft X-ray intensity for ≥M2 soft X-ray flares from 1995 to 2005 located at longitudes from E120°–E41°. Solid circles represent flares associated with SWPC SEP events. The black thick contour indicates the probability threshold used in the analysis.

would correspond to the end of the third 5-min interval with J (>10 MeV) ≥ 10 pfu). However, as *Posner* [2007] has recently shown, the GOES >10 MeV SEP time profiles are affected by contamination from relativistic electrons/protons during the SEP onset period. Thus, we did not use the GOES >10 MeV SEP data to determine onset times for the 47 successful forecasts ("hits") made (post hoc) by our technique for solar cycle 23, but instead used the 31–50 MeV proton onset times published by *Posner* [2007] for 19 of these 47 events. For the 19 common events, we obtain delay times ranging from −7 min to 882 min with a median of 39 min. For comparison, for these events Posner obtained a range from 13 min to 727 min (median = 35 min). Note that the onset times obtained by Posner refer not to the NOAA event threshold crossing (or equivalent at 31–50 MeV) but rather to the rise of the event above the preevent background. Even for very fast rise events, the required 15-min interval above threshold to confirm a NOAA SEP event indicates that advance warning (with a range of 8 min to 897 min and a median of 54 min) would have been issued for all 19 events by our technique.

4. Discussion

4.1. Recently Developed SEP Warning Techniques

[40] The current emphasis on solar system exploration and the attendant radiation threat to astronauts have resulted in increased emphasis on SEP event forecasting. With "advanced (physics-based) predictive models" lying "a number of years in the future" [*Baker et al.*, 2007], empirical models or decision aids such as that presented here will have to bridge the gap. Several articles [*Kubo and Akioka*, 2004; *Garcia*, 2004a, 2004b; *Posner*, 2007; *Balch*, 2008] have focused on such techniques. How do the feasibility and performance of the method presented here compare with that of the techniques presented in these recent articles?

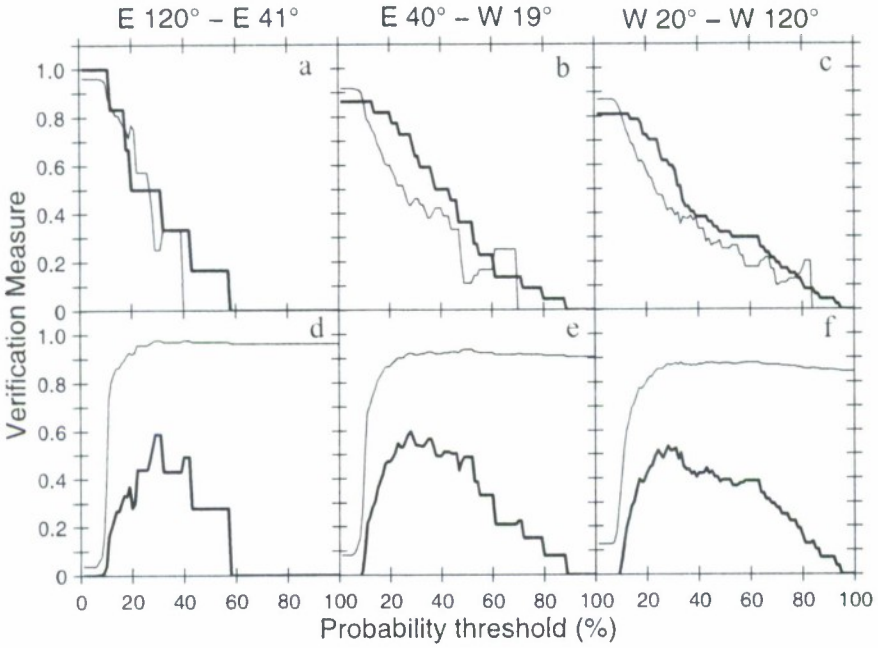

Figure 10. SEP event forecast performance based on probability thresholds. POD (thick line) and FAR (thin line) as functions of the probability threshold for (a) eastern, (b) intermediate, and (c) western events. HSS (thick line) and PC (thin line) as functions of the probability threshold for (d) eastern, (e) intermediate, and (f) western events.

[41] 1. *Kubo and Akioka* [2004] showed that for both solar cycles 22 and 23, an integrated SXR flux of ~20 ergs cm^{-2} was an almost necessary condition (POD ~100%) for a disk flare to be followed by an SWPC SEP event. They note that while 400 SXR flares had time-integrated fluxes of ~20 ergs cm^{-2} since 1997, only 60 SWPC SEP events occurred during this time, indicating a high (~85%) false alarm rate if this method was used by itself.

[42] 2. *Garcia* [2004a] used a combination of SXR flare peak intensity and peak flare temperature (given by the ratio of the 0.5–3 Å SXR flux to the 1–8 Å flux [*Garcia*, 1994b]). For the optimum method based on these two parameters, and additional constraints based on flare duration and flare location, the reported POD was 94% (46/49) and the FAR was 46% (39/85). If, however, we calculate the POD as was done for our technique, i.e., taking into account all SWPC SEP events associated with disk SXR flares of any size, then the POD drops to 58% (46/80).

[43] 3. *Garcia* [2004b] used the hard X-ray spectral index (as determined by the NOAA/Czech HXRS experiment [*Farník et al.*, 2001]) as an input parameter for SEP prediction and obtained a POD of 88% (14/16) and a FAR of 18% (3/17) from March 2000 through December 2002. However, SWPC SEP events associated with disk flares too weak (≤M1.9) to permit spectral analysis were not considered as missed events (nine such SEP events occurred during the interval used, see Table 1) and 11 SXR flares (many with the flat spectral signature associated with SEP events) that occurred when a SEP event was still in progress were not considered in the analysis. Both of these effects will degrade the performance of the *Garcia* [2004b] hard X-ray technique. That said, *Kiplinger* [1995] reported comparable results (POD = 96% (22/23) and FAR = 27% (8/30)) for a similar prediction method based on hard X-ray spectra, indicating promise for this approach.

[44] 4. Most recently, *Posner* [2007] explored the use of relativistic electrons as precursors for >30 MeV proton events (see *Kuwabara et al.* [2006] for a ground level event (>500 MeV protons) alarm system based on neutron monitor data). The method was developed for 1996–2002 and tested for year 2003, during which it predicted 4 of 5 SEP events (POD = 80%) with a FAR of 56% (5/9), although, as discussed by the author, there are mitigating factors for several of the false alarms. For the year 2003,

Table 3. Contingency Matrix for Evaluating the Forecast Model[a]

	Event Observed: Yes	Event Observed: No
Event Forecast: Yes	A = 47	B = 34
Event Forecast: No	C = 16 (+12)	D = 586

[a]The numbers (excluding the 12 SEP events associated with <M2 flares) do not add to 704 because of missing SXR or radio data for 21 events.

our method (evaluated as above for SWPC threshold events) yielded comparable results, with a POD of 87% (7/8) and a FAR of 46% (6/13). The difference in the number of threshold SEP events (5 for *Posner* [2007] versus 10 in our Table 1) is due to *Posner* [2007] use of the 30–50 MeV channel on the Comprehensive Suprathermal and Energetic particle Analyzer (COSTEP) instrument on SOHO rather than the GOES >10 MeV channel and a higher event trigger intensity threshold (~20 pfu versus 10 pfu). Because of the different SEP database on which the *Posner* [2007] technique was developed, a direct comparison of it with our method is not possible; we can state that the two methods give comparable results for the SEP energies and event thresholds for which they were developed.

4.2. Standardization

[45] The above review/comparison highlights the need for standardized databases and definitions for SEP warning studies. Standardized comparisons are required if space weather forecasting is to follow the path of steady incremental improvement that has characterized progress in terrestrial weather forecasting [*Siscoe*, 2006].

[46] Our first suggestion is to use a standardized database for testing new algorithms. Toward this end, we have included both our SEP event and SXR data (in the auxiliary material) bases, as Table 1 and Data Set S1, respectively. Thus anyone wishing to improve on our technique can compare results based on the same sample of events, in order to verify gains.

[47] Our second suggestion is standardizing protocols for identifying hits, misses, and false alarms. For example, in this study:

[48] 1. We used a "one SEP event, one flare" association rule, with the credited solar event being the one that took the SEP event across the ≥10 pfu threshold. This is necessary because a "yes/no" SWPC SEP event decision needs to be made for each "triggering" flare (i.e., ≥M2) in our scheme.

[49] 2. We issued a hypothetical forecast for every soft X-ray event that met our ≥M2 threshold, regardless of flare location (frontside/backside, observed/inferred) and the SEP background intensity at the time of the flare. If no Hα flare was reported in association with a ≥M2 flare, we made our best guess as to the origin based, e.g., on active region flare histories, and issued a (post hoc) yes/no prediction, because this is what the duty forecaster would need to do. For a particle based technique such as that of *Posner* [2007], the triggering event would not be a flare but an electron (or high-energy proton event) above a certain threshold.

[50] 3. We required an increase of a factor of two to register a hit when the triggering ≥M2 flare occurred when the SEP intensity was already above the SWPC event threshold. If such an increase was not achieved following a positive forecast, a false alarm was registered. This approach differs from that used by SWPC (K. Doggett, personal communication, 2007). If the SEP intensity at the time of a new (triggering) flare is already above threshold, SWPC will not issue a new (positive or negative) forecast, although the end time of the event in progress may be extended. Our procedure will yield a greater number of hits and false alarms.

[51] 4. We counted all SEP events associated with <M2 disk flares as misses (even though no forecast was attempted).

[52] 5. We ignored small (<M2) behind the limb events for which the input data may have been compromised. This limitation may not apply to all techniques, e.g., the electron-based technique of *Posner* [2007]. In such cases, techniques should be evaluated on an equal footing with special events such as these treated the same in the evaluation of all methods being compared.

[53] Our final suggestion is that new forecast methods should determine the delay from the time of forecast to the >10 MeV onset (data permitting) for comparison with existing techniques (see the discussions of warning lead times given by *Garcia* [2004a] and *Posner* [2007]).

4.3. Current Objective Techniques for SEP Event Forecasting: Moving Beyond 50–50

[54] *Cliver et al.* [1985] reported that the U-shaped microwave burst criterion for predicting SWPC SEP events [*Castelli et al.*, 1967] had both POD and FAR of ~50% for the 1965–1979 time interval. When one considers that by raising and lowering the SXR prediction threshold in a given technique (say from C1 to X10 in our scheme), one can force results ranging from POD ~100% and FAR ~100% to POD ~0% and FAR ~0%, 50/50 represents the baseline starting point for progress. The technique presented in this study yielded a POD of 63% and a FAR of 42% (for the years on which it was developed). These results, as well as all those for the other recent studies discussed above (with the possible exception of the hard X-ray technique of *Garcia* [2004b]), pale in comparison with the current, forecaster-in-the-loop, method currently in use at SWPC.

[55] The reason for this is that the forecaster brings both experience and more observations to the task. Note that all of the above techniques involve at the most three variables including, generally, a measure of flare size and location. Generally speaking, the more data brought to bear on a forecast, the better the result. For example, a simple two-dimensional plot of integrated SXR intensity (from the SXR fluence used information in Data Set S1) versus flare longitude yields a FAR of 64% for a POD of 63%, a poorer result than that obtained when the third input parameter (integrated radio flux) was considered. None of the techniques discussed here takes into account the SEP history of a given region. Given the tendency for SEP events to occur in clusters [e.g., *Švestka*, 1968; *Cliver*, 1980], such knowledge will figure prominently in the forecaster's evaluation of a flare which exceeds the SEP forecast trigger threshold. Other factors such as the SEP background flux near Earth at the time of a flare may also play

a role [*Cliver*, 2006; *Mewaldt et al.*, 2006]. And combined methods using both flare electromagnetic and particle input also offer promise, particularly for SEP events originating from behind-the-limb flares where occultation effects compromise electromagnetic emissions. Until the performance of objective methods, either empirical or physics-based, exceeds those of the "forecaster-in-the-loop" model, however, the use of such techniques is necessarily relegated to that of a decision aid.

[56] **Acknowledgments.** Part of the work by M.L. and M.S. was performed under COST 724 Action and part under the ASI contract I/090/06/0. E.W.C. was supported through the Window on Europe program of the European Office of Aerospace Research and Development. We acknowledge a helpful discussion with Kent Doggett of the SWPC.

References

Baker, D. N., et al. (2007), Space radiation hazards and the vision for space exploration: A report on the October 2005 Wintergreen conference, *Space Weather*, *5*, S02004, doi:10.1029/2007SW000313.

Balch, C. C. (1999), SEC proton prediction model: Verification and analysis, *Radiat. Meas.*, *30*, 231–250, doi:10.1016/S1350-4487(99)00052-9.

Balch, C. C. (2006), An updated statistical prediction model for solar energetic particles: New approaches, paper presented at Solar Heliospheric and Interplanetary Environment Workshop, Midway, Utah, 31 Jul. to 4 Aug.

Balch, C. C. (2008), Updated verification of SEC's solar energetic particle prediction model, *Space Weather*, *6*, S01001, doi:10.1029/2007SW000337.

Beck, P., M. Latocha, S. Rollet, and G. Stehno (2005), TEPC reference measurements at aircraft altitudes during a solar storm, *Adv. Space Res.*, *36*(9), 1627–1633, doi:10.1016/j.asr.2005.05.035.

Belov, A., H. Garcia, V. Kurt, H. Mavromichalaki, and M. Gerontidou (2005), Proton enhancements and their relation to the X-ray flares during the three last solar cycles, *Sol. Phys.*, *229*, 135–139, doi:10.1007/s11207-005-4721-3.

Bougeret, J.-L., et al. (1995), Waves: The Radio and Plasma Wave Experiment on the Wind spacecraft, *Space Sci. Rev.*, *71*, 231–263, doi:10.1007/BF00751331.

Cane, H. V., R. E. McGuire, and T. T. von Rosenvinge (1986), Two classes of solar energetic particle events associated with impulsive and long-duration soft X-ray flares, *Astrophys. J.*, *301*, 448–459, doi:10.1086/163913.

Cane, H. V., D. V. Reames, and T. T. von Rosenvinge (1988), The role of interplanetary shocks in the longitude distribution of solar energetic particles, *J. Geophys. Res.*, *93*, 9555–9567, doi:10.1029/JA093iA09p09555.

Cane, H. V., W. C. Erickson, and N. P. Prestage (2002), Solar flares, type III radio bursts, coronal mass ejections, and energetic particles, *J. Geophys. Res.*, *107*(A10), 1315, doi:10.1029/2001JA000320.

Cane, H. V., R. A. Mewaldt, C. M. S. Cohen, and T. T. von Rosenvinge (2006), Role of flares and shocks in determining solar energetic particle abundances, *J. Geophys. Res.*, *111*, A06S90, doi:10.1029/2005JA011071.

Castelli, J. P., J. Aarons, and G. A. Michael (1967), Flux density measurements of radio bursts of proton-producing flares and nonproton flares, *J. Geophys. Res.*, *72*, 5491–5498, doi:10.1029/JZ072i021p05491.

Cliver, E. W. (1980), Almost-necessary conditions for a solar active region to produce a subsequent polar cap absorption event, *Tech. Rep. AFGL-TR-80-0151*, Air Force Geophys. Lab., Hanscom Air Force Base, Mass.

Cliver, E. W. (2006), The unusual relativistic proton events of 1979 August 21 and 1981 May 10, *Astrophys. J.*, *639*, 1206–1217, doi:10.1086/499765.

Cliver, E. W., and A. G. Ling (2007), Electrons and protons in solar energetic particle events, *Astrophys. J.*, *658*, 1349–1356, doi:10.1086/511737.

Cliver, E. W., S. W. Kahler, and P. S. McIntosh (1983), Solar proton flares with weak impulsive phases, *Astrophys. J.*, *264*, 699–707, doi:10.1086/160643.

Cliver, E. W., L. F. McNamara, and L. C. Gentile (1985), Peak flux density spectra of large solar radio bursts and proton emission from flares, *J. Geophys. Res.*, *90*, 6251–6266, doi:10.1029/JA090iA07p06251.

Cliver, E. W., S. W. Kahler, and D. V. Reames (2004), Coronal shocks and solar energetic proton events, *Astrophys. J.*, *605*, 902–910, doi:10.1086/382651.

Cohen, C. M. S., R. A. Mewaldt, A. C. Cummings, R. A. Leske, E. C. Stone, P. L. Slocum, M. E. Wiedenbeck, E. R. Christian, and T. T. von Rosevinge (2001), Forecasting the arrival of shock-accelerated solar energetic particles at Earth, *J. Geophys. Res.*, *106*, 20,979–20,983, doi:10.1029/2000JA000216.

Croom, D. L. (1971a), Solar microwave bursts as indicators of the occurrence of solar proton emission, *Sol. Phys.*, *19*, 152–170, doi:10.1007/BF00148831.

Croom, D. L. (1971b), Forecasting the intensity of solar proton events from the time characteristics of solar microwave bursts, *Sol. Phys.*, *19*, 171–185, doi:10.1007/BF00148832.

Cucinotta, F., G. Badwahr, P. Saganti, W. Schimmerling, J. Wilson, L. Peterson, and J. Dicello (2002), Space radiation cancer risk projections for exploration missions: Uncertainty reduction and mitigation, *Rep. NASA/TP 2002-210777*, NASA Johnson Space Cent., Houston, Tex.

Dyer, C., F. Lei, A. Hands, S. Clucas, and B. Jones (2005), Measurements of the atmospheric radiation environment from CREAM and comparisons with models for quiet time and solar particle events, *IEEE Trans. Nucl. Sci.*, *52*(6), 2326–2331, doi:10.1109/TNS.2005.860754.

Dyer, C. S., K. Hunter, S. Clucas, and A. Campbell (2004), Observation of the solar particle events of October and November 2003 from CREDO and MPTB, *IEEE Trans. Nucl. Sci.*, *51*(6), 3388–3393, doi:10.1109/TNS.2004.839156.

Fárník, F., H. Garcia, and M. Karlický (2001), New solar broad-band hard X-ray spectrometer: First results, *Sol. Phys.*, *201*, 357–372, doi:10.1023/A:1017533125731.

Feynman, J., and S. B. Gabriel (2000), On space weather consequences and predictions, *J. Geophys. Res.*, *105*, 10,543–10,564, doi:10.1029/1999JA000141.

Garcia, H. A. (1994a), Temperature and hard X-ray signatures for energetic proton events, *Astrophys. J.*, *420*, 422–432, doi:10.1086/173572.

Garcia, H. A. (1994b), Temperature and emission measure from GOES soft X-ray measurements, *Sol. Phys.*, *154*, 275–308, doi:10.1007/BF00681100.

Garcia, H. A. (2004a), Forecasting methods for occurrence and magnitude of proton storms with solar soft X-rays, *Space Weather*, *2*, S02002, doi:10.1029/2003SW000001.

Garcia, H. A. (2004b), Forecasting methods for occurrence and magnitude of proton storms with solar hard X-rays, *Space Weather*, *2*, S06003, doi:10.1029/2003SW000035.

Getley, I. L., M. L. Duldig, D. F. Smart, and M. A. Shea (2005), The applicability of model based aircraft radiation dose estimates, *Adv. Space Res.*, *36*(9), 1638–1644, doi:10.1016/j.asr.2005.09.011.

Hargreaves, J. K. (2005), A new method of studying the relation between ionization rates and radio-wave absorption in polar-cap absorption events, *Ann. Geophys.*, *23*(2), 359–369.

Heckman, G. R. (1979), Predictions of the Space Environment Services Center, in *Solar-Terrestrial Predictions Proceedings*, vol. 1, edited by R. F. Donnelley, pp. 322–349, U. S. Dep. of Commer., Washington, D. C.

Hoff, J. L., L. W. Townsend, and E. N. Zapp (2004), Interplanetary crew doses and dose equivalents: Variations among different bone marrow and skin sites, *Adv. Space Res.*, *34*(6), 1347–1352, doi:10.1016/j.asr.2003.08.056.

Hunsucker, R. D. (1992), Auroral and polar-cap ionospheric effects on radio propagation, *IEEE Trans. Antennas Propag.*, *40*(7), 818–828, doi:10.1109/8.155747.

Iucci, N., et al. (2005), Space weather conditions and spacecraft anomalies in different orbits, *Space Weather*, *3*, S01001, doi:10.1029/2003SW000056.

Kahler, S. W. (1982), The role of the big flare syndrome in correlations of solar energetic proton fluxes and associated microwave burst parameters, *J. Geophys. Res.*, *87*, 3439–3448, doi:10.1029/JA087iA05p03439.

Kahler, S. W., M. A. Shea, D. F. Smart, and E. W. Cliver (1991), Ground-level events from impulsive solar flares, *Conf. Pap. Int. Cosmic Ray Conf. 22nd*, *3*, 21–24.

Kahler, S. W., E. W. Cliver, and A. G. Ling (2007), Validating the proton prediction system (PPS), *J. Atmos. Sol. Terr. Phys.*, *69*, 43–49, doi:10.1016/j.jastp.2006.06.009.

Kiplinger, A. L. (1995), Comparative studies of hard X-ray spectral evolution in solar flares with high-energy proton events observed at Earth, *Astrophys. J.*, *453*, 973–986, doi:10.1086/176457.

Klein, K.-L., S. Krucker, G. Trottet, and S. Hoang (2005), Coronal phenomena at the release of solar energetic electron events, *Astron. Astrophys.*, *431*, 1047–1060, doi:10.1051/0004-6361:20041258.

Kocharov, G. E., G. A. Kovaltsov, and L. G. Kocharov (1983), Generation of accelerated particles and hard radiation during solar flare, *Conf. Pap. Int. Cosmic Ray Conf. 18th*, *4*, 105–108.

Kubo, Y., and M. Akioka (2004), Existence of thresholds in proton flares and application to solar energetic particle alerts, *Space Weather*, *2*, S01002, doi:10.1029/2003SW000022.

Kuwabara, T., J. W. Bieber, J. Clem, P. Evenson, and R. Pyle (2006), Development of a ground level enhancement alarm system based upon neutron monitors, *Space Weather*, *4*, S10001, doi:10.1029/2006SW000223.

Lario, D. (2005), Advances in modelling gradual solar energetic particle events, *Adv. Space Res.*, *36*(12), 2279–2288, doi:10.1016/j.asr.2005.07.081.

Laurenza, M., J. Hewitt, E. W. Cliver, M. Storini, and A. Ling (2007), Solar energetic proton events and soft X-ray flares, paper presented at 20th Eur. Cosmic Ray Symp. 2006, Lisbon 5–8 Sept. (Available online at http://www.lip.pt/events/2006/ecrs/proc/ecrs06-s1-34.pdf.)

Leblanc, Y., G. A. Dulk, and J.-L. Bougeret (1998), Tracing the electron density from the corona to 1 AU, *Sol. Phys.*, *183*, 165–180, doi:10.1023/A:1005049730506.

MacDowall, R. J., A. Lara, P. K. Manoharan, N. V. Nitta, A. M. Rosas, and J. L. Bougeret (2003), Long-duration hectometric type III radio bursts and their association with solar energetic particle (SEP) events, *Geophys. Res. Lett.*, *30*(12), 8018, doi:10.1029/2002GL016624.

Marque, C., A. Posner, and K.-L. Klein (2006), Solar energetic particles and radio-silent fast coronal mass ejections, *Astrophys. J.*, *642*, 1222–1235, doi:10.1086/501157.

McCracken, K. G. (1962), The cosmic-ray flare effect: 3. Deductions regarding the interplanetary magnetic field, *J. Geophys. Res.*, *67*, 447–458, doi:10.1029/JZ067i002p00447.

McCullagh, P., and J. A. Nelder (1983), *Generalized Linear Models*, chap. 4, pp. 98–155, Chapman and Hall, London.

Mewaldt, R. A., G. M. Mason, C. S. Cohen, A. C. Cummings, M. I. Desai, R. A. Leske, E. C. Stone, T. T. von Rosevinge, and M. E. Wiedenbeck (2006), Dependence of solar energetic particle intensities on the density of suprathermal seed particles, paper presented at 36th Committee on Space Research Scientific Assembly, Beijing, 16–23 Jul.

National Geophysical Data Center (2006), Solar-geophysical data, report, Boulder, Colo.

Nonnast, J. H., T. P. Armstrong, and J. W. Kohl (1982), A study of solar flare soft X-rays and their relation to particle events observed with IMP 8, *J. Geophys. Res.*, *87*, 4327–4337, doi:10.1029/JA087iA06p04327.

Posner, A. (2007), Up to 1-hour forecasting of radiation hazards from solar energetic ion events with relativistic electrons, *Space Weather*, *5*, S05001, doi:10.1029/2006SW000268.

Reames, D. V. (1999a), Particle acceleration at the Sun and in the heliosphere, *Space Sci. Rev.*, *90*, 413–491, doi:10.1023/A:1005105831781.

Reames, D. V. (1999b), Solar energetic particles: Is there time to hide?, *Radiat. Meas.*, *30*(3), 297–308, doi:10.1016/S1350-4487(99)00066-9.

Roussev, I. I., I. V. Sokolov, T. G. Forbes, T. I. Gombosi, M. A. Lee, and J. J. Sakai (2004), A numerical model of a coronal mass ejection: Shock development with implications for the acceleration of GeV protons, *Astrophys. J.*, *605*, L73–L76, doi:10.1086/392504.

Sarris, E. T., and S. D. Shawhan (1973), Characteristics of electron and high-energy proton flares, *Sol. Phys.*, *28*, 519–532, doi:10.1007/BF00152322.

Shea, M. A., and D. F. Smart (1990), A summary of major solar proton events, *Sol. Phys.*, *127*, 297–320, doi:10.1007/BF00152170.

Siscoe, G. (2006), A culture of improving forecasts: Lessons from meteorology, *Space Weather*, *4*, S01003, doi:10.1029/2005SW000178.

Smart, D. F., and M. A. Shea (1979), PPS76: A computerized event mode solar proton forecasting technique, in *Solar-Terrestrial Predictions Proceedings*, vol. 1, edited by R. F. Donnelley, pp. 406–427, NOAA, Washington, D. C.

Smart, D. F., and M. A. Shea (1989), PPS-87—A new event oriented solar proton prediction model, *Adv. Space Res.*, *9*(10), 281–284, doi:10.1016/0273-1177(89)90450-X.

Smart, D. F., and M. A. Shea (1992), Modeling the time-intensity profile of solar flare generated particle fluxes in the inner heliosphere, *Adv. Space Res.*, *12*(2–3), 303–312, doi:10.1016/0273-1177(92)90120-M.

Sokolov, I. V., I. I. Roussev, L. A. Fisk, M. A. Lee, T. I. Gombosi, and J. I. Sakai (2006), Diffusive shock acceleration theory revisited, *Astrophys. J.*, *642*, L81–L84.

Švestka, Z. (1968), On long-term forecasts of proton flares, *Sol. Phys.*, *4*, 18–29, doi:10.1007/BF00146995.

Tylka, A. J., C. M. S. Cohen, W. F. Dietrich, M. A. Lee, C. G. Maclennan, R. A. Mewaldt, and C. K. Ng (2005), Elemental composition at high energies in large gradual solar particle events, *Astrophys. J.*, *625*, 474–495, doi:10.1086/429384.

Van Hollebeke, M. A. I., L. S. Ma Sung, and F. B. McDonald (1975), The variation of solar proton energy spectra and size distribution with heliolongitude, *Sol. Phys.*, *41*, 189–223, doi:10.1007/BF00152967.

Webber, W. R. (1963), A review of solar cosmic ray events, in *AAS-NASA Symposium on the Physics of Solar Flares*, edited by W. N. Hess, pp. 215–255, NASA, Washington, D. C.

Wright, C. S. (1980), On the longitudinal distribution of solar type II bursts, *Proc. Astron. Soc. Aust.*, *4*, 59–61.

Zank, G. P., G. Li, G. M. Webb, J. A. Le Roux, V. Florinski, X. Ao, and W. K. M. Rice (2005), Particle acceleration at collisionless shocks: An overview, in *AIP Conf. Proc.*, vol. *781*, pp. 170–179.

C. C. Balch, NOAA Space Weather Prediction Center, 325 Broadway, Boulder, CO 80305, USA.

E. W. Cliver and J. Hewitt, Space Vehicles Directorate, AFRL, Hanscom Air Force Base, MA 01731-3010, USA.

M. L. Kaiser, NASA Goddard Space Flight Center, Mail Code 130, Greenbelt, MD 20771, USA.

M. Laurenza and M. Storini, Institute of Interplanetary Space Physics, INAF, Via del Fosso del Cavaliere 100, Rome I-00133, Italy. (monica.laurenza@ifsi-roma.inaf.it)

A. G. Ling, Atmospheric Environmental Research, Inc., 131 Hartwell Avenue, Lexington, MA 02421-3136, USA.